HHS Public Access

Author manuscript

Nat Neurosci. Author manuscript; available in PMC 2024 June 24.

Published in final edited form as:

Nat Neurosci. 2024 January ; 27(1): 90–101. doi:10.1038/s41593-023-01504-3.

A pontomesencephalic PACAPergic pathway underlying panic-like behavioral and somatic symptoms in mice

Sukjae J. Kang[1,5], **Jong-Hyun Kim**[1,4,5], **Dong-Il Kim**[1], **Benjamin Z. Roberts**[1,2], **Sung Han**[1,2,3,*]

[1]Peptide Biology Laboratory, The Salk Institute for Biological Studies, La Jolla, CA, USA.

[2]Neuroscience Graduate Program, University of California, San Diego, La Jolla, CA, USA.

[3]Center for Neuroscience Imaging Research, Institute for Basic Science and Department of Biomedical Engineering, Sungkyunkwan University, Suwon, 16419, Republic of Korea.

[4]Current address: Center for Cognition and Sociality, Institute for Basic Science, Daejeon, 34126, Republic of Korea.

[5]These authors contributed equally to this work (Alphabetical order).

Abstract

Panic disorder is characterized by uncontrollable fear accompanied by somatic symptoms that distinguish it from other anxiety disorders. Neural mechanisms underlying these unique symptoms are not completely understood. Here we report that the pituitary adenylate cyclase-activating polypeptide (PACAP)-expressing neurons in the lateral parabrachial nucleus projecting to the dorsal raphe (DR) are crucial for panic-like behavioral and physiological alterations. These neurons are activated by panicogenic stimuli but inhibited in conditioned fear and anxiogenic conditions. Activating these neurons elicits strong defensive behaviors and rapid cardiorespiratory increase without creating aversive memory, whereas inhibiting them attenuates panic-associated symptoms. Chemogenetic or pharmacological inhibition of downstream PACAP receptor-expressing DR neurons abolishes panic-like symptoms. The pontomesencephalic PACAPergic pathway is therefore a likely mediator of panicogenesis, and may be a promising therapeutic target for treating panic disorder.

Anxiety disorders constitute the most common class of psychiatric diseases, encompassing posttraumatic stress disorder, generalized anxiety disorder, phobic disorders, and panic disorder[1]. Patients with panic disorder experience recurrent spontaneous panic attacks, which begin with feelings of uncontrollable fear and/or distress and rapidly progress to

*Corresponding author. sunghan@salk.edu.

Author Contributions:
Conceptualization: SH, JHK, SJK
Methodology: SH, JHK, SJK
Investigation: JHK, SJK
Visualization: JHK, SJK
Funding acquisition: SH
Virus provision: DIK
Writing: SH, JHK, SJK, BR

Competing Interests: The authors declare no competing interests.

severe autonomic symptoms (e.g., palpitation, hypertension, dizziness, nausea, vomiting, abdominal discomfort)[2–4]. This combination of unconditioned fear and somatic symptoms distinguishes panic disorder from other anxiety disorders. Previous neuroanatomical studies have proposed several candidate brain regions for panic disorder pathogenesis, including the amygdala, thalamus, hypothalamus, periaqueductal gray, locus coeruleus, and lateral parabrachial nucleus (PBL)[5,6]. While the amygdala is often considered to be a likely primary mediator of panic disorder given its role in the fear response and panic attacks[7–9], studies of patients with bilateral amygdala lesions revealed that this structure is not necessary for fear induction and panicogenesis following CO_2 inhalation[10–12]. The PBL regulates autonomic functions (e.g., cardiorespiratory activity, body temperature), relays multimodal aversive sensory signals to the amygdala[13–16], and, compellingly, coordinates breathing rate with anxiety[17]. Furthermore, the PBL is activated by panicogenic conditions in rodents[18,19], and possibly in humans[20,21]. The PBL is therefore a promising candidate for the neural substrate of panicogenesis. However, studies have yet to identify the specific neuronal populations and circuit configurations that underlie panicogenesis.

Pituitary adenylate cyclase-activating polypeptide (PACAP, encoded by the gene *Adcyap1*) is expressed abundantly in the PBL (Allen Brain Atlas, experiment 74511882), and mediates stress-induced behavioral and physiological responses[22–26]. Furthermore, human studies showed that epigenetic and genetic alterations in the *ADCYAP1* and *ADCYAP1R1* genes (the latter encoding the PACAP type 1 receptor; PAC1R) are associated with panic disorder[27,28]. Therefore, we hypothesize that PBL PACAP neurons are crucial for panic-specific behavioral and somatic symptoms in mice.

Using cell type- and projection-specific circuit monitoring, manipulation, and mapping techniques, we report that PBL PACAP neurons projecting to the dorsal raphe nucleus (DR) ($PACAP^{PBL\rightarrow DR}$) are activated by panicogenic stimuli (i.e., 10% CO_2 and the β-carboline $GABA_A$ receptor inverse agonist, FG-7142[29]) and inhibited by anxiogenic stimuli and conditioned fear. Activating these neurons evoked robust defensive behaviors and strong cardiorespiratory activation without forming associative fear memory. Inhibiting these neurons themselves or their downstream PAC1R-expressing target neurons in the DR blocked the behavioral and autonomic responses to panicogenic conditions in mice. These findings delineate a novel neural mechanism underlying panic-specific behavioral and somatic symptoms, which may facilitate the identification of therapeutic targets for the treatment of panic disorder.

RESULTS

Opposing $PACAP^{PBL\rightarrow DR}$ neural responses to panicogenic and anxiogenic stimuli

The PBL is connected to many regions of the brain, including those involved in fear/anxiety and autonomic functions[13]. We expressed EYFP specifically in $PACAP^{PBL}$ neurons by stereotaxically injecting an AAV that expresses EYFP in a Cre-dependent fashion (AAV-DIO-EYFP) into the PBL of $Adcyap1^{Cre/+}$ mice. EYFP localization revealed that $PACAP^{PBL}$ neurons innervate the central nucleus of the amygdala (CeA), the bed nucleus of the stria terminalis (BNST), and the DR (Extended Data 1a,b). To determine whether the same neurons collaterally project to all three areas, we labeled $PACAP^{PBL}$ neurons in

a projection-specific manner. We injected retrograde AAV viruses that express mCherry or EYFP in a Cre-dependent manner (retroAAV-DIO-mCherry and retroAAV-DIO-EYFP) into the CeA and DR, respectively (Fig. 1a). Interestingly, the two fluorescent signals did not overlap in the PBL, indicating that two distinct populations of $PACAP^{PBL}$ neurons project divergently to different downstream areas. Dorsal lateral $PACAP^{PBL}$ neurons project to the DR ($PACAP^{PBL\rightarrow DR}$), and external lateral $PACAP^{PBL}$ neurons project to the CeA ($PACAP^{PBL\rightarrow CeA}$) and presumably to the BNST[30]. Previous studies have shown that the PBL PACAP neurons projecting to the CeA and BNST are involved in both anxiety-like behavior and pain perception[31,32]. However, given that humans with bilateral amygdala lesions still experience fear induction and panicogenesis during CO_2 inhalation[10–12], we sought to investigate the as-yet undetermined role of DR-projecting $PACAP^{PBL}$ neurons in panic-like behaviors.

To monitor the response of $PACAP^{PBL\rightarrow DR}$ neurons to various behavioral conditions, we labeled $PACAP^{PBL\rightarrow DR}$ neurons in a projection-specific manner by delivering two AAV vectors into the *Adcyap1*$^{Cre/+}$ mice. First, a Cre-dependent retroAAV encoding Flp-recombinase (retroAAV-DIO-FlpO) was injected unilaterally into the DR, resulting in the expression of Flp-recombinase in $PACAP^{PBL}$ neurons projecting to the DR. Then, an AAV that expresses GCaMP6s in a Flp-dependent manner (AAV-fDIO-GCaMP6s) was injected unilaterally into the PBL, resulting in the expression of GCaMP6s in $PACAP^{PBL\rightarrow DR}$ neurons labeled with FlpO. An optic ferrule was implanted in the PBL of these same mice (Fig. 1b). Three weeks later, these mice were subjected to panicogenic conditions and calcium activity of $PACAP^{PBL\rightarrow DR}$ neurons was monitored with fiber photometry (Fig. 1c–l).

CO_2 challenge is a well-established experimental model for panic in both animal models and patients with panic disorder[33–35]. Animals were subjected to a two-day paradigm consisting of a habituation period (day 1) followed by exposure to 10% CO_2 or regular air (day 2; Fig. 1c). As reported previously[33,34], mice exposed to 10% CO_2 for 10 min traveled less distance in the testing arena than control mice exposed to air (Extended Data 2a). Mice exposed to 10% CO_2 also exhibited marked immobile behavior compared with controls (Fig. 1d) (note that we use the term “immobility” to describe non-moving behaviors in response to panicogenic conditions, while the term “freezing” will refer to a more typical defensive behavior in response to electric foot shock). Monitoring $PACAP^{PBL\rightarrow DR}$ neuronal activity during these tests revealed a robust increase in activity during 10% CO_2 exposure (Fig. 1e). Given that hyperventilation is a well-known symptom of a panic attack in humans[2–4], we also used collar sensors to monitor respiratory activity in a separate cohort of mice. We observed elevations in breathing and heart rate followed by a decrease in heart rate during the 10 min of 10% CO_2 exposure (Fig. 1f,g). The observed sequence of heightened breathing and heart rate followed by a decrease in heart rate during the 10% CO_2 exposure can be a physiological response of the mice to regulate their respiratory and cardiovascular systems in the presence of elevated CO_2 levels.

Next, we monitored the activity of $PACAP^{PBL\rightarrow DR}$ neurons in mice during pharmacologically-induced panicogenesis (Fig. 1h). We used FG-7142—a complex anxiogenic/panicogenic drug previously used in panic studies to produce anxiety-like

behaviors and the somatic symptoms of a panic attack in humans[36] and animals[29,37–41]__ and compare it with other panicogenic or anxiogenic conditions. As previously reported, FG-7142 dramatically reduced locomotor activity (Extended Data 2b) and increased immobility (Fig. 1i) relative to control solution during the 1-h observation period[38]. After around 20–25 min, the FG-7142 injected mice exhibited increased PACAP$^{PBL\rightarrow DR}$ activity (Fig. 1j), with breathing and heart rates following a similar pattern (Fig. 1k,l)[29,37].

We next monitored the calcium activity of PACAP$^{PBL\rightarrow DR}$ neurons in conditioned fear and anxiogenic conditions (Fig. 2, Extended Data 3, 4). First, a cohort of mice was subjected to an auditory fear conditioning paradigm in which a neutral tone was associated with a foot shock stimulus (Fig. 2a). Foot shock during the conditioning period gradually increased freezing behavior across trials (Fig. 2b). PACAP$^{PBL\rightarrow DR}$ neurons were robustly activated by foot shock (Extended Data 3a). Foot shock-conditioned animals demonstrated high levels of freezing during context-dependent and cue-dependent fear memory tests (Fig. 2c,d), in conjunction with a gradual decrease in PACAP$^{PBL\rightarrow DR}$ neuronal activity in both conditions (Fig. 2e,h). While the heart rate was slightly increased, the breathing rate decreased in a similar manner as the calcium signal (Fig. 2f,g,i,j). No changes in neuronal activity were observed in non-foot shock controls.

The PBL is well-known as a general alarm center[42], and we recently reported that CGRP-expressing PBL neurons were activated by multi-modal aversive sensory stimuli[43]. To examine whether these neurons are also activated by other aversive sensory stimuli, mice were subjected to a looming stimulus, a well-known visual threat stimulus. Interestingly, PACAP$^{PBL\rightarrow DR}$ neuronal activity was decreased in response to the looming disk (Extended Data 3b). Additionally, PACAP$^{PBL\rightarrow DR}$ neuronal activity was inhibited during the elevated platform assessment (Extended Data 4a,b) and when the animals entered the open arm of the elevated plus-maze (Extended Data 4c–e). Thus, PACAP$^{PBL\rightarrow DR}$ neuronal activity was downregulated by conditioned fear and anxiogenic conditions.

Collectively, these data reveal that PACAP$^{PBL\rightarrow DR}$ neurons respond differentially to various types of aversive conditions. Although panicogenic conditions produced a similar behavioral outcome (i.e., immobility) as conditioned fear (i.e., freezing), both PACAP$^{PBL\rightarrow DR}$ neuronal activity and breathing rate were elevated by panicogenic stimuli but lowered in fear and anxiogenic conditions. These divergent neural and respiratory responses imply that the two types of conditions engage fundamentally different neural and physiological mechanisms and that PACAP$^{PBL\rightarrow DR}$ neurons may be part of a panic-specific circuit.

To identify inputs to PACAP$^{PBL\rightarrow DR}$ neurons, we performed cTRIO (**c**ell-type-specific **T**racing of the **R**elationship between **I**nput and **O**utput) projection-specific input/output mapping. Presynaptic cells were predominantly observed in the BNST and CeA. The results of the immunostaining of brain slices containing these regions suggest that PACAP$^{PBL\rightarrow DR}$ neurons primarily receive monosynaptic input from non-GABAergic neurons of the BNST and GABAergic neurons of the CeA (Extended Data 5).

Activating PACAP$^{PBL→DR}$ neurons produces panic-like symptoms

To directly assess the extent to which PACAP$^{PBL→DR}$ neurons contribute to the behavioral and physiological symptoms of panicogenesis, we monitored behavioral and cardiorespiratory changes during optogenetic manipulation of these neurons. For optogenetic manipulations, we bilaterally injected retroAAV-DIO-FlpO into the DR, resulting in Flp-recombinase expression in PACAP^{PBL} neurons projecting to the DR. Then, an AAV expressing ChR2 in a Flp-dependent manner (AAV-fDIO-ChR2-EYFP) was bilaterally injected into the PBL. In this way, ChR2 was expressed in PACAP$^{PBL→DR}$ neurons labeled with FlpO (Fig. 3a). At the same time, optic ferrules were bilaterally implanted into the PBL of these mice.

We first investigated whether activation of PACAP$^{PBL→DR}$ neurons generates aversive memory as previously observed by stimulating the PBL→CeA pathway[14]. Briefly, mice were trained in a modified classical auditory fear conditioning paradigm in which a 30-sec tone (conditioned stimulus) was paired with a 10-sec burst of photostimulation (unconditioned stimulus) instead of a foot shock (Fig. 3b). Photostimulation of ChR2-expressing PACAP$^{PBL→DR}$ neurons instantly caused the mice to become immobile. This immobility persisted even after the laser was turned off (Fig. 3c, Supplementary Video1). This effect was not observed in EYFP control mice (Supplementary Video 2). The following day we performed context- and cue-dependent memory tests by exposing the mice to either the same or a novel chamber and delivering the same conditioned stimulus. ChR2 and control groups exhibited very low levels of immobility during both tests (Fig. 3d,e, Supplementary Videos 3,4), indicating that activation of these neurons produced strong defensive behaviors but did not create an associative fear memory.

Since photostimulation induced persistent immobility during conditioning, we next sought to determine whether PACAP$^{PBL→DR}$ neurons encode negative valence using a real-time place aversion (RTPA) paradigm (Fig. 3f). We used 2-sec bursts of photostimulation instead of continuous illumination to avoid persistent immobility, as it interfered with the assessment (see Methods for details). ChR2-expressing mice spent substantially less time in the stimulation-paired chamber than control mice and actively retreated from the paired chamber when the laser was on (Fig. 3g,h). These results demonstrate that photostimulating PACAP$^{PBL→DR}$ neurons produced immediate defensive responses, but not context- or cue-dependent fear memories.

We next sought to determine whether photoactivation of PACAP$^{PBL→DR}$ neurons could evoke panic-like physiological responses. Optogenetic activation of these neurons frequency-dependently evoked strong immobility and tail rattling behaviors (Supplementary Video 5), accompanied by dramatic increases in breathing and heart rate as recorded by pulse oximeter and neck sensor (Fig. 3i,j). In summary, optogenetic activation of PACAP$^{PBL→DR}$ neurons immediately induced robust aversive behaviors accompanied by increased cardiorespiratory activity.

To confirm that these effects were due to manipulations of specifically the PACAP$^{PBL→DR}$ circuit, we repeated the above experiments while photostimulating axon terminals rather than somas. We bilaterally injected AAV-DIO-ChR2-EYFP into the PBL, resulting in ChR2

expression in PACAP^{PBL} neurons. Then, optic ferrules were bilaterally implanted above the DR (Fig. 4a). Photostimulation of PACAP$^{PBL\rightarrow DR}$ axon terminals produced the same effects in the modified auditory fear conditioning paradigm (Fig. 4b) as somatic activation (Fig. 3b–e)—i.e., immobility (Fig. 4c) without formation of associative fear memory (Fig. 4d,e). The results of RTPA experiments were also identical across photostimulation conditions (Fig. 3f–h, 4f–h), supporting our above finding that the PACAP$^{PBL\rightarrow DR}$ circuit encodes negative valence. Finally, axon terminal activation increased breathing and heart rate (Fig. 4i,j), similarly to cell body activation (Fig. 3i,j). These data demonstrate that the PACAP$^{PBL\rightarrow DR}$ pathway encodes behavioral and physiological responses that are associated specifically with panicogenic stimuli.

Inhibiting PACAP$^{PBL\rightarrow DR}$ neurons reduces panic-like symptoms

Given that the activity of PACAP$^{PBL\rightarrow DR}$ neurons increased in response to panicogenic conditions, we next asked whether chemogenetic inhibition of these neurons would affect the behavioral and autonomic responses to 10% CO_2. We expressed AAV-EF1α-fDIO-hM4Di-mCherry in the PBL of *Adcyap1*$^{Cre/+}$ mice using a procedure similar to that used for the optogenetics experiments (Fig. 5a). We next monitored locomotor activity following i.p. injections of the DREADD agonist CNO (3 mg/kg) under 10% CO_2 and control conditions. Whereas exposure to 10% CO_2 decreased locomotor activity in the mCherry control group relative to normal air (as previously observed), CO_2 did not differentially affect the locomotion of the hM4Di group versus air (Fig. 5b,c, Extended Data 6a). We then investigated whether inhibition of PACAP$^{PBL\rightarrow DR}$ neurons could attenuate the behavioral and physiological responses to the anxiogenic/panicogenic agent, FG-7142. I.p. injection of FG-7142 decreased locomotion (Fig. 5d,e, Extended Data 6b,c) and increased cardiorespiratory rates (Fig. 5f,g) in control mice. CNO attenuated these responses in the hM4Di group but not the control group. These results indicate that activation of PACAP$^{PBL\rightarrow DR}$ neurons is necessary for pharmacologically induced panic-like behavioral and somatic symptoms.

Downstream PAC1R^{DR} neurons are necessary for panicogenesis

The PACAP receptor (PAC1R, encoded by the *Adcyap1r1* gene) is abundantly expressed in the DR (Allen Brain Atlas, experiment 74988667). This led us to hypothesize that PAC1R-expressing DR neurons are direct functional targets of PACAP$^{PBL\rightarrow DR}$ neurons and contribute to panicogenesis. A retrograde rabies virus strategy was used on PAC1R^{DR} neurons to confirm this monosynaptic connection (Fig. 6a, Extended Data 7). The results of the RNAscope *in situ* hybridization with PACAP (*Adcyap1*), VGluT2 (*Slc17a6*), and VGAT (*Slc32a1*) mRNAs in PBL slices of these same mice show that the PBL neurons directly projecting to the PAC1R^{DR} neurons are co-labelled with the PACAP and VGluT2, but not VGAT, indicating that the glutamatergic PACAP^{PBL} neurons make monosynaptic connections to the PAC1R^{DR} neurons (Fig. 6b,c).

To evaluate the role of PAC1R^{DR} neurons in panic-like behaviors, we chemogenetically inhibited this population and monitored behavioral and autonomic changes induced by panicogenic stimuli (namely, 10% CO_2 or FG-7142). We bilaterally injected AAV-hSyn-DIO-hM4Di-mCherry into the DR of *Adcyap1r1*$^{Cre/+}$ mice (Fig. 6d). Consistent with

our PACAP$^{PBL\rightarrow DR}$ inhibition experiment, treating hM4Di-expressing mice with CNO blocked the locomotor and cardiorespiratory responses to panicogenic conditions, compared with controls (Fig. 6e–j, Extended Data 8). Next, we optogenetically activated PAC1R^{DR} neurons with ChR2 (Fig. 6k) to determine whether similar results could be produced from PACAP$^{PBL\rightarrow DR}$ circuit activation. Activating PAC1R^{DR} neurons reproduced the immediate immobility behavior (Fig. 6l, Supplementary Video 6) and breathing rate increase following circuit activation (Fig. 6m), although heart rate was affected differently (Fig. 6n). Finally, we administered a PAC1R antagonist before assessment in panicogenic conditions to further confirm the function of PAC1R^{DR} neurons. Acute pharmacological inhibition of PAC1R signaling in the DR by cannular infusion of PACAP(6–38) (Fig. 7a) attenuated behavioral responses induced by CO_2 (Fig. 7b–d) or FG-7142 (Fig. 7e–h). These results indicate that PACAP signaling from PACAP^{PBL} to PAC1R^{DR} neurons is indispensable for behavioral and autonomic responses induced by panicogenic stimuli.

Excessive serotonin signaling is strongly associated with panic disorder pathology [44–46], which, given the above findings, could reflect an alteration of DR serotonergic output by PACAP$^{PBL\rightarrow DR}$ input. We performed *in situ* hybridization to detect *Adcyap1r1* gene expression in the DR of the Ai14:*Slc6a4*$^{Cre+}$ mice, in which serotonin transporter (SERT)-expressing neurons are labeled with tdTomato. We found that ~98% of PAC1R-expressing neurons were SERT-positive (Extended Data 9). PAC1R^{DR} neurons with Cre-dependent expression of ChR2-EYFP revealed that these neurons innervate to well-known projection targets of DR serotonergic neurons[47,48] and send especially strong projections to the peri-locus coeruleus (peri-LC) area of the brainstem (Extended Data 10)[49]. These results indicate that the PACAP$^{PBL\rightarrow DR}$ pathway induces panic-like symptoms by recruiting a novel population of PAC1R-expressing serotonergic neurons within the DR.

DISCUSSION

We report that PACAP$^{PBL\rightarrow DR}$ neurons were robustly activated by panicogenic stimuli but, surprisingly, were inhibited by anxiogenic and conditioned fear stimuli (Fig. 1, 2, Extended Data 2,3). These results demonstrate that conditioned fear/anxiety and panic are distinct behavioral manifestations induced by threat, and that PACAP$^{PBL\rightarrow DR}$ neurons encode panic-specific signals. Although conditioned fear and panicogenic stimuli produced similar behavioral output in mice (i.e., freezing/immobility), we suggest that these conditions engage distinct fundamental mechanisms given the observed differences in cardiorespiratory and PACAP$^{PBL\rightarrow DR}$ neuronal activity. Photostimulation of these neurons evoked strong defensive behaviors (immobility and tail rattling[50,51]) and cardiorespiratory activation but did not create associative fear memories (Fig. 3,4). This observation is consistent with the unique features of panic disorder, namely unconditioned fear accompanied by physical symptoms. Chemogenetic inhibition of PACAP$^{PBL\rightarrow DR}$ neurons or PAC1R-expressing postsynaptic partners in the DR completely blocked the behavioral and physiological changes induced by panicogenic conditions. Furthermore, the delivery of PAC1R antagonist into the DR attenuated panic-like symptoms. Taken together, these findings demonstrate that the PACAP$^{PBL\rightarrow DR}$ signaling pathway mediates panic disorder-specific behavioral and somatic symptoms. Therefore, the PACAP^{PBL} → PAC1R^{DR} signaling pathway is an ideal target for novel therapeutic interventions for panic disorder[52].

Our results indicate that the PACAP$^{PBL\rightarrow DR}$ pathway is both necessary and sufficient for the induction of panic-like symptoms. Our cTRIO input/output mapping revealed that PACAP$^{PBL\rightarrow DR}$ neurons receive modulatory input from GABAergic neurons of the CeA and non-GABAergic neurons of the BNST. The CeA is comprised solely of GABAergic neurons[53] and plays critical roles in fear and anxiety[54]. CeA GABAergic firing rate increases in response to conditioned fear[55]; therefore, activation of these neurons may drive the suppression of PACAP$^{PBL\rightarrow DR}$ activity observed in conditioned fear/anxiogenic conditions (Fig. 2, Extended Data 3). In contrast, decreased inhibitory input from the CeA to PACAP$^{PBL\rightarrow DR}$ neurons under certain conditions may increase susceptibility to panic. Indeed, GABAergic dysfunction is strongly associated with depression and anxiety disorders[56,57], and individuals with these conditions are more likely to experience panic attacks[58–60]. Therefore, we speculate that decreased GABAergic input from CeA to PACAP$^{PBL\rightarrow DR}$ neurons in depression and anxiety disorders may increase the risk of panic attacks.

Recent findings indicate that the BNST, a limbic structure broadly implicated in behavioral responses to stressor exposure and anxiety[61] but not fear-like defensive responses to threats[62,63], may play an important role in CO_2-evoked behavioral responses[64]. Although the PBL directly receives hypercapnic signals from central chemoreceptors[65,66], previous studies and our findings suggest that the PBL may also receive CO_2-evoked signals from the BNST. Patients with bilateral amygdala lesions can experience fear and panic responses triggered by hypercapnia, suggesting that the amygdala is not essential for inducing fear and panic through CO_2 inhalation[10–12]. However, it is possible that the amygdala plays a critical role in other aspects of panic disorder. For instance, panic disorder is often accompanied by agoraphobia, which involves avoiding open spaces to prevent spontaneous panic attack, indicating the associative fear memory component of panic disorder[67,68]. Patients with bilateral amygdala lesions are incapable of forming associative fear memory of exteroceptive threat cues. Although it is uncertain whether hypercapnia acts as an unconditioned stimulus to form associative fear memory, it is likely that the amygdala is responsible for the aversive memory of panic attacks. Our study demonstrates that the PACAP^{PBL} → PAC1R^{DR} peptidergic circuit is necessary and sufficient for CO_2-induced panicogenesis but is not involved in associative fear memory formation. These findings indicate that this PACAPergic panicogenesis pathway is part of a distributed network of multiple brain areas that mediates panic-induced behavioral, physiological, and emotional changes. Taken together, our results suggest that the PACAP^{PBL}→PAC1R^{DR} circuit initiates panic-like behavioral and somatic symptoms in response to hypercapnic condition. Future research on the function of the CeA/BNST input neurons may offer more detailed insights into the circuit-based mechanism of panic and fear/anxiety interactions.

The PBL is known for its role as a general alarm center that relays multi-modal aversive sensory stimuli, including pain[42,43,69,70]. Our results show that PACAP$^{PBL\rightarrow DR}$ neurons are activated by hypercapnic condition (10% CO_2) and acute painful stimulus (0.2 mA electric footshock), but inhibited by visual threat (looming stimulus), conditioned fear, and anxiety. It is interesting to note that aversive stimuli originating from the body that directly damage the body activate these neurons, whereas threat signal originating from outside the body, or from the memory of previous threat exposure inhibit these neurons. This suggests that

the PACAP$^{PBL\rightarrow DR}$ neurons are part of PBL general alarm system and have a specialized role in detecting interoceptive aversive signals that directly harm the body. Previous studies have shown that optogenetic stimulation of PBL glutamatergic neurons induces negative valence[70] and escaping behaviors such as running and jumping, but no freezing behavior[69]. However, we showed that photostimulation of glutamatergic PACAP$^{PBL\rightarrow DR}$ neurons encodes negative valence with immediate immobility and tail rattling, further supporting the idea that these neurons are a subset of general alarm-encoding neurons that has unique functions different from other PBL glutamatergic populations. Notably, photostimulation of these neurons induced immediate defensive behaviors, such as freezing and tail rattling, while panicogenic stimuli, such as 10% CO_2 and FG-7142, triggered defensive states with slower temporal dynamics. In response to CO_2 inhalation, neuronal activation and associated behavioral/somatic changes were observed approximately 1 minute after exposure, while in response to i.p. injection of FG-7142, they were observed approximately 30 minutes later. These temporal differences in the defensive state dynamics are likely due to the different mechanisms by which these stimuli activate the PACAP$^{PBL\rightarrow DR}$ neurons. While optogenetic stimulation directly activated these neurons, activation of these neurons by panicogens required multiple steps. Furthermore, the temporal difference in defensive response between CO_2 and FG-7142 is mainly due to their distinct action mechanisms. CO_2 rapidly activates central chemoreceptor neurons, which in turn activate the PACAP neurons in the PBL. In contrast, FG-7142 acts by inhibiting the $GABA_A$ receptor in parabrachial neurons including PACAP$^{PBL\rightarrow DR}$ neurons[19] and must first cross the blood-brain barrier. Taken together, these findings suggest that distinct stimuli can elicit defensive responses with different temporal scales due to differences in their mechanisms of action on the PACAP$^{PBL\rightarrow DR}$ neurons. It is important to consider these differences when interpreting the defensive response to various stimuli.

Based on clinical and experimental evidence, Deakin and Graeff have proposed that different serotonergic pathways originating from the DR play distinct roles in anxiety and panic[71]; specifically, orbital frontal cortex-projecting DR serotonin neurons promote active coping behavior, whereas CeA-projecting neurons mediate anxiety-like behaviors[47]. Moreover, the DR serotonergic population innervating the dorsal periaqueductal gray and rostroventrolateral medulla inhibits the escape response in the presence of imminent danger, and is presumably the primary mediator of the panicolytic effect of selective serotonin reuptake inhibitors[48,72–74]. Optogenetic or chemogenetic activation of DR serotonergic neurons produces variable locomotor effects, meanwhile, differentially decreasing overall activity[47,75,76] or changing movement speed[77] in some situations but not others[78]. Furthermore, pharmacological inhibition of DR 5-HT_{2B} receptors suppressed cocaine-induced hyperlocomotion[79], and lesioning the DRN with the serotonergic neurotoxin 5,7-dihydroxytryptamine had no effect on phencyclidine-induced hyperlocomotion[80]. These divergent results indicate considerable anatomical and functional heterogeneity of DR serotonergic neurons. The PAC1R^{DR} neurons, which are mostly serotonergic (Extended Data 6), share some of the previously defined characteristics of DR serotonergic populations. However, these neurons also have distinct functional properties. Chemogenetic inhibition of PAC1R^{DR} neurons abolished the behavioral and somatic effects of panicogenic conditions, while photostimulation of these neurons immediately reproduced these effects

(i.e., increased immobility and breathing rate). The decrease in heart rate produced by photostimulation of $PAC1R^{DR}$ neurons was unexpected, although previous studies show that either i.c.v. administration of serotonin[81] or activation of 5-HT_{1A} receptors in the DR[82] decreased heart rate. A pharmacological study also shows that activation of DR can reduce heart rate[83]. It is also known that increased serotonin can activate 5-HT_{1A} autoreceptors that inhibit serotonergic neurons in the DR[84,85]; however, the role of $PAC1R^{DR}$ neurons in the regulation of 5-HT_{1A} receptor-mediated functions has yet to be studied.

Finally, acute delivery of a PAC1R antagonist, PACAP(6–38), into the DR attenuated behavioral changes evoked by panicogenic stimuli. In light of the lack of progress in the development of panic-specific medications[86], these $PAC1R^{DR}$ neurons, representing a novel serotonergic population within the DR, may serve as a potential target for the treatment of panic disorder. This potential may be expanded upon via the characterization of the functional properties of panic disorder-relevant downstream circuits. The findings of a recent study suggest that the external lateral parabrachial nucleus (PBel) is functionally downstream of the DR serotonergic neurons that mediates hypercapnic arousal[87]. Inhibiting the $Sert^{DR}\rightarrow CGRP^{PBel}$ pathway reduces arousal by hypercapnic condition during sleep. Notably, the $CGRP^{PBel}$ neurons and $PACAP^{PBL\rightarrow DR}$ neurons are spatially separated distinct PBL subpopulation, indicating that they constitute an indirect reciprocal connection of $PACAP^{PBL}\rightarrow PAC1R/SERT^{DR}\rightarrow CGRP^{PBel}$ circuit. Similar indirect reciprocal connections are also present among the CeA and BNST within the PBL. Although their functional role is not yet fully understood, these reciprocal connections may form feedback circuits that modulate the primary function of the PBL.

Together, our results demonstrate that $PACAP^{PBL\rightarrow DR}$ and $PAC1R^{DR}$ neurons form a novel pontomesencephalic pathway that underlies behavioral and somatic responses induced by panicogenic stimuli. The comprehensive series of experiments reported in this analysis has revealed a novel unconditioned fear circuit critical for the induction of panic-specific behavioral and somatic symptoms in mice. Importantly, our findings provide the first evidence that panic-like symptoms can be attenuated by pharmacological blockade of PBL→DR PACAP signaling in mice, a discovery that may aid the development of novel therapeutic interventions for panic disorder.

Materials and Methods

Animals

All protocols for animal experiments were approved by the IACUC of the Salk Institute for Biological Studies according to NIH guidelines for animal experimentation. The *Adcyap1*$^{Cre/+}$ (Strain #030155), *Adcyap1r1*$^{Cre/+}$ (Strain #035572), Ai14 (Strain #007914), *Slc6a4*$^{Cre/+}$ (Strain #014554) and C57Bl/6J (Strain #000664) mouse lines were obtained from the Jackson laboratory. All mouse lines were backcrossed with C57Bl/6J for > 6 generations. Male and female mice were used in all studies. Animals were randomized to experimental groups, and no sex differences were noted. Mice were maintained on a standard 12-hour light/dark cycle in a temperature- (20–22 °C) and humidity- (45–55%) controlled vivarium and provided with food and water *ad libitum*.

Stereotaxic surgery for virus injection and optic fiber implantation

Mice were anesthetized by isoflurane gas anesthesia (induction at 3.5%, and maintenance at 1.5–2%, the Dräger Vapor® 2000; Draeger), and then placed on a stereotaxic frame (David Kopf Instruments). Holes were drilled with a micromotor handpiece drill (Foredom) after the exposure of the skull. Viruses were injected using a pulled fine-glass capillary (3–000-203-G/X, Drummond Scientific) connected to a Microliter syringe (84850, Hamilton) with Tygon tubing. The syringe was placed on an infusion pump (70–2002, Harvard Apparatus) for a steady injection rate of 0.05 μL/min. Unilateral (right side) and bilateral injections were made for the following target regions: PBL (anteroposterior (AP), −5.1 mm; mediolateral (ML), 1.35 mm; dorsoventral (DV) −3.5 mm from bregma), DR (AP, −4.6mm; ML, 0.3mm; DV, −3.35mm) and CeA (AP, −1.05mm; ML, 2.8mm; DV, −4.6 mm). A total volume of 0.3 or 0.5 μL of the virus was injected, and the fine-glass capillary was slowly removed from the injection site seven minutes after injection.

For determining the outputs of $PACAP^{PBL}$ or $PAC1R^{DR}$ neurons, 0.3 μL of AAV-EF1a-DIO-EYFP (2.12E+12 GC/mL) was injected into the PBL of *Adcyap1*$^{Cre/+}$ or DR of *Adcyap1r1*$^{Cre/+}$ transgenic mice. Mice were sacrificed four weeks after the injection.

For tracing the inputs to $PACAP^{PBL}$ neurons, 0.5 μL of retroAAV-DIO-mCherry (1.51E+13 GC/mL) and retroAAV-DIO-EYFP (5E+12 GC/mL) were injected into, respectively, the CeA and DR of *Adcyap1*$^{Cre/+}$ transgenic mice. Mice were sacrificed three weeks after the injection.

For monitoring $PACAP^{PBL\rightarrow DR}$ neurons via fiber photometry, 0.3 μL of retroAAV-DIO-FlpO-WPRE-hGHpA (1.98E+13 GC/mL) was injected unilaterally into the DR of *Adcyap1*$^{Cre/+}$ transgenic mice, and 0.3 μL of AAV8-fDIO-GCaMP6s-EYFP (1.0E+13 GC/mL) was injected into the PBL. A custom-made stainless-steel mono fiber-optic cannula (400 μm, 0.37 NA) was implanted above the PBL (0.2 mm above virus injection coordinate). Two screws were implanted away from the injection site as anchors. Superglue and dental cement were used to fix the implantation. Experiments took place three weeks after injection.

For cTRIO tracing, 0.3 μL of retroAAV-DIO-FlpO-WPRE-hGHpA was first injected unilaterally into the DR, then 0.3 μL of AAV8-CAG-fDIO-TVA-mCherry (1.0E+12 GC/mL) and AAV8-CAG-fDIO-oG-WPRE-SV40PA (2.25E+12 GC/mL) was injected into the PBL. Three weeks later, 0.3 μL of EnvA G-deleted Rabies-eGFP (1.03E+09 GC/mL) was injected into the same PBL location. Mice were sacrificed five days after the final injection.

For retrograde rabies tracing, 0.3 μL AAV8-hSyn-FLEX-TVA-P2A-GFP-2A-oG (3.82E+12 GC/mL; Salk Institute viral vector core) was injected into the DR of *Adcyap1r1*$^{Cre/+}$ transgenic mice. After 2 weeks, 0.3 μL of EnvA-ΔG-rabies-mCherry (3.95E+08 GC/mL; Salk Institute viral vector core) was injected into the same region. Mice were sacrificed five days after the final injection.

For optogenetic activation of $PACAP^{PBL\rightarrow DR}$ neurons, 0.3 μL of retroAAV-DIO-FlpO-WPRE-hGHpA was injected bilaterally into the DR of *Adcyap1*$^{Cre/+}$ transgenic mice, and

0.3 μL of AAV9-EF1a-fDIO-hChR2(H134R)-EYFP (5.21E+12 GC/mL) or AAV8-EF1a-fDIO-EYFP (4.39E+12 GC/mL) was injected into the PBL. Custom-made ceramic mono fiber-optic cannulas (200 μm, 0.22 NA) were implanted above the PBL (0.2 mm above virus injection coordinate). Experiments took place three weeks after injection.

For optogenetic axon terminal activation of $PACAP^{PBL}$ neurons projecting to DR, 0.3 μL of AAVDJ-EF1a-DIO-hChR2(H134R)-EYFP-WPRE-pA (4.5E+12 GC/mL) or AAV-EF1a-DIO-EYFP was injected bilaterally into the PBL of *Adcyap1*$^{Cre/+}$ transgenic mice. Custom-made ceramic mono fiber-optic cannulas (200 μm, 0.22 NA) were implanted above the DR (0.2 mm above virus injection coordinate). Experiments took place three weeks after injection.

For optogenetic activation of $PAC1R^{DR}$ neurons, 0.3 μL of AAVDJ-EF1a-DIO-hChR2(H134R)-EYFP-WPRE-pA or AAV-EF1a-DIO-EYFP was injected bilaterally into the DR of *Adcyap1r1*$^{Cre/+}$ transgenic mice. Custom-made ceramic mono fiber-optic cannulas (200 μm, 0.22 NA) were implanted above the DR (0.2 mm above virus injection coordinate at a 15° angle). Experiments took place three weeks after injection and cannula implantation.

For chemogenetic inhibition of $PACAP^{PBL\rightarrow DR}$ neurons, 0.3 μL of retroAAV-DIO-FlpO-WPRE-hGHpA was injected bilaterally into the DR, and 0.3 μL of AAVDJ-hSyn-fDIO-hM4Di-mCherry (1.98E+13 GC/mL) or AAV8-EF1a-fDIO-EYFP into the PBL of *Adcyap1*$^{Cre/+}$ transgenic mice. Experiments took place three weeks after injection.

For chemogenetic inhibition of $PAC1R^{DR}$ neurons, 0.3 μL of AAVDJ-EF1a-DIO-hM4Di-mCherry (6.04E+11 GC/mL) or AAV-EF1a-DIO-EYFP was injected into the DR of *Adcyap1r1*$^{Cre/+}$ transgenic mice. Experiments took place three weeks after injection.

For pharmacology experiments, an internal cannula (8IC315GMNSPC, P1 Technologies Inc., USA) was connected with a dummy cannula (8IC315FDMN02, P1 Technologies Inc., USA) and implanted bilaterally into the DR at a 15° angle (AP, −4.6mm; ML, 1.14mm; DV, −3.45mm). Experiments took place one week after the implantation.

Fiber photometry

Bulk calcium signals from $PACAP^{PBL\rightarrow DR}$ neurons were monitored using a custom-built fiber photometry system based on the open-source pyPhotometry platform (https://pyphotometry.readthedocs.io/en/latest/). A 465 nm LED was used to induce Ca^{2+}-dependent fluorescence signals, and a 405 nm LED was used for Ca^{2+}-independent (isosbestic) fluorescence signals. Motion-corrected ΔF/F was calculated post-hoc using the formula: $\Delta F/F = F_{465} - F_{405fit} / F_{405fit}$ for the whole experimental time. The least-squares polynomial function was used to calculate F_{405fit}. There was no normalization for experiments that are shown with no baseline (Fig. 1e, 2e, Extended Data 4). Fiberphotometry results that have a stable initial phase or baseline were normalized by the mean value of those period to align near 0 (5 s for Extended Data 3b; 30 s for Fig. 2h, Extended Data 3a; 10 min for Fig. 1j). Area under the curve (AUC) was used to analyze the data.

Physiology

MouseOx ®-Plus oximeter (STARR Life Sciences Corp.) was used to measure the breathing and heart rates of mice. Mouse necks were shaved and the collar sensor (Size XS) was applied. Animals were habituated to the collar sensor for 1–2 days before experiments. Data were collected through MouseOx ®-Plus Software attached to the computer.

CO_2 exposure test

A custom-built open-bottom plexiglass chamber (28 × 28 × 32 cm) was used to monitor panic-like behavior during CO_2 exposure. Normal air and 10% CO_2 gas tanks were connected with Tygon tubing with a Y-shaped connector, and the other end was inserted into a hole in the wall of the chamber. A thick layer of cage cover paper was used to thoroughly seal the bottom of the chamber. The chamber was enclosed in a light- and sound-attenuating cubicle (ENV-018MD, MED Associates).. Normal air was infused for 10–20 min at a rate of 4 l/min, followed by 10% CO_2 for 10 or 30 min (only the PAC1R^{DR}::hM4Di and their control group was exposed for 30 min due to their resistance to CO_2). All trials were recorded by a USB camera (DFK 33GX236, Imagine Source) attached to the computer, and behaviors were analyzed by video-tracking software (EthoVision XT 12, Noldus). Immobility was analyzed during the last 10 min of the "before CO_2" period (air) and the entirety (10 or 30 min) of the "after CO_2" period by setting the "not moving" factor as 1.25–1.5cm/s, for 3s samples in Ethovision. For physiological data collection, mice were connected with collar sensors and placed inside the chamber with air exposure. 10% CO_2 was injected 30–50 min after collar sensor attachment.

FG-7142 injection

FG-7142 (20 mg/kg, i.p., #0554, Tocris) was injected to induce panic-like symptoms. For fiber photometry and behavior tracking, mice were placed inside a standard mouse cage. Injections were performed 10 min after habituation. All trials were recorded by a USB camera attached to the computer, and behaviors were analyzed byEthovision. Immobility was analyzed in 20 min bins by setting the "not moving" factor as 1.25–1.5cm/s, for 3s samples in Ethovision. For physiological data collection, mice were connected with collar sensors and placed inside a non-transparent glass cylinder (15 cm diameter with 20 cm height) with bedding. FG-7142 was injected 30–50 min after collar sensor attachment. Data are presented from 5 mins after the injection to exclude the effect of injection-related discomfort.

Fear conditioning test

A fear conditioning chamber (26 × 30 × 33 cm, ENV-007CT, MED Associates) with a metal grid floor (ENV-005, MED Associates) connected to a standalone aversive electric shock stimulator (ENV-414S, MED Associates) was used for foot shock (unconditioned stimulus; US) delivery. A USB camera was connected to a computer, and Ethovision was used for shock delivery and behavioral analysis. Two speakers (AX210, Dell) were placed beside the chamber for the delivery of conditioned stimuli (CS+). The chamber was enclosed in a light- and sound-attenuating cubicle. The chamber was cleaned with 70% ethanol and double-distilled water between each trial. During habituation, mice were placed

inside the chamber and allowed to explore for 2 min (baseline). The CS+ (30 sec, 2 kHz pure tone) was then delivered six times with random inter-stimulus intervals. Mice were returned to the same context on day 2. After 1 min of baseline exploration, mice received 5 2-sec foot shocks (0.2 mA, US) co-terminating with CS+ at random inter-event intervals. Non-conditioned control mice did not receive foot shocks. On day 3, mice were fitted with either an optic fiber for fiber photometry or a collar sensor for physiological measurements. Mice were then re-introduced to the same context for 3 min for the context test. 6 hr later, mice were fitted with an optic fiber or collar sensor and introduced to a new context for the cue test (a glass cylinder wrapped with a non-transparent material; 20 cm diameter, 15 cm height); the 30-sec CS+ was then delivered three times without the US. All trials were recorded by a USB camera attached to the computer, and controlled by Ethovision. Freezing behavior was manually scored by experienced experimenters in a blinded manner. In manual scoring, the time of immobility of the mouse without any movement except breathing was counted as freezing behavior[88,89].

Looming test

Mice were habituated in a standard mouse cage for 10 min. After habituation, an expanding looming stimulus (2-s, 3- or 9-inch diameter) was delivered with an LED screen facing the arena from above.

Elevated platform test

A cup or clear circular platform (diameter is 100 mm) was fixed to the top of a camera tripod (1 m tall). Mice were habituated for 15 min in a cup before being placed on the platform for 5 min.

Elevated plus maze test

A custom-built elevated plus maze with two transparent closed arms (35 × 7 × 30 cm) and two open arms (35 × 7 × 2 cm) was used to monitor anxiety-like behavior in mice. The maze was elevated 70 cm from the floor for all tests. Mice were placed on the end of the open arm facing the center of the maze. Behavior was recorded for 10 min and quantified using Ethovision. Both 70% ethanol solution and deionized water were used to clean the maze immediately after each trial.

Optogenetic conditioning test

The procedure was the same as that described in the ‘Fear conditioning test’ section, with the exception that optogenetic stimulation was used as the US instead of foot shock. Optic fibers were connected bilaterally to the optic ferrules on the mouse’s head during habituation and conditioning. During conditioning, mice received 6 10-sec bursts of 470 nm laser photostimulation (LRD-0470-PFFD-00100–05, LaserGlow Tech; 20 Hz, 4 ms pulse, 8–9 mW intensity) co-terminated with CS+ (random inter-event intervals). 4-ms laser pulse width was used to minimize retrograde action potentials from the DR afferent stimulation during the axon terminal photostimulation experiment. On day 3, context and cue tests were performed without an optic fiber connection. All trials were recorded by a USB camera attached to the computer, and immobility behavior was analyzed by Ethovision.

Real-time place aversion (RTPA)

A two-chamber arena (30 × 60 × 30 cm) was used for the RTPA test. Behavior was tracked with a USB camera using Ethovision. PACAP$^{PBL\rightarrow DR}$::ChR2 mice were connected with optic fibers and randomly placed on one side of the chamber or the other. Modified photostimulation parameters (2 sec of 4-ms pulsed 20 Hz stimulation with 10-sec inter-trial intervals) were used to prevent immobility. The laser was activated when a mouse entered the chamber adjacent to the one in which it was originally placed and turned off when it returned to the original chamber. Sessions lasted 20 min.

Photostimulation for physiological recording

A glass cylinder arena (15 cm diameter with 20 cm height) was used for the test. Mice were habituated for 30–50 min inside the arena after collar sensor and optic fiber connection. Four different frequencies (5, 10, 20, and 40 Hz) of 470 nm laser photostimulation were given to PACAP$^{PBL\rightarrow DR}$::ChR2 mice for 5 sec in 60-sec intervals. 40 Hz photostimulation (7 mW) was given to PAC1R^{DR}::ChR2 mice for 5 sec. The laser pulse width was 4 ms for all conditions.

PAC1R^{DR}::ChR2 photostimulation

PAC1R^{DR}::ChR2 mice were habituated in a standard mouse cage for 10 min, and 40 Hz (4 ms pulse width, 10-sec exposure, 7 mW) of 470 nm laser was given to monitor the behavioral change.

Chemogenetics

Experiments were performed 10 min after CNO injection (3 mg/kg, i.p.; #16882, Cayman chemical, USA).

Pharmacology

Mice were anesthetized by isoflurane gas for drug infusion. Internal cannulas were connected to Microliter syringes with Tygon tubing. The syringe was placed on an infusion pump for a steady injection rate of 0.05 μL/min. Internal cannulas were inserted into guide cannulas after removing dummy cannulas. 1 μg of PAC1R antagonist PACAP (6–38) (3236, Tocris, USA) or control solution was infused bilaterally into the DR. The internal cannulas were removed 2 min after infusion, and experiments took place at least 10 min after the mice woke up.

In situ hybridization

Following rapid decapitation of Ai14; *Slc6a4*$^{Cre/+}$ (SERT-Ai14) or rabies virus injected *Adcyap1r1*$^{Cre/+}$ transgenic mice, brains were frozen in −50 °C iso-methylbutane with OCT compound and stored at −80 °C. Coronal sections containing DR regions that corresponded to the injection plane used in the behavioral experiments were cut in 20 μm-thick slices for SERT-Ail4 at −20 °C and thaw-mounted onto slides. Coronal sections containing DR or PBL regions were cut in 10 μm-thick slices for PAC1R^{DR} retrograde rabies tracing at −20 °C and thaw-mounted onto slides. *In situ* hybridization was performed according to the RNAScope 2.0 Fluorescent Multiple Kit User Manual for Fresh Frozen Tissue (Advanced

Cell Diagnostics, Inc., USA). Slides containing the specified coronal brain slices were fixed in 4% paraformaldehyde, dehydrated, and pretreated with protease IV solution for 30 min for SERT-Ai14 and 12 min for rabies virus injected *Adcyap1r1*$^{Cre/+}$ transgenic mice. Slices were then incubated with either target probes for mouse *Adcyap1r1* (accession number NM_001025372.1, probe region 4108 – 5038), Mm-*Adcyap1* (RNAScope Probe #405911, Advanced Cell Diagnostics), Mm-*Slc17a6* (RNAScope probe #319171-C3, Advanced Cell Diagnostics) or Mm-*Slc32a1* (RNAScope probe #319191-C3, Advanced Cell Diagnostics) for 2 hr. Following probe hybridization, slices underwent a series of probe signal amplification steps (AMP1–4). SERT-Ai14 underwent a final incubation of fluorescently labeled probes (Alexa 488) designed to target the specified channel associated with the probes. Slides were counterstained with DAPI, and coverslips were mounted with Vectashield Hard Set mounting medium (Vector Laboratories).

Histology and immunohistochemistry

Mice were intracardially perfused with 4% paraformaldehyde in PBS (phosphate buffered saline). Brains were kept in 4% PFA overnight for post-fixation and dehydrated in 30% sucrose for 1–2 days before sectioning. Frozen brains were cut into 50 μm coronal slices with a cryostat and stored in PBS before mounting. Brain tissues were mounted on a slide glass (12–550-143, Fisher Scientific, USA) with a DAPI-containing mounting solution (0100–20, SouthernBiotech).

For the cTRIO experiment, every slice 100 μm apart was mounted for counting (n = 3 mice).

For immunohistochemistry with the cTRIO mice, coronal slices containing BNST or CEA were washed with PBST (Phosphate buffered saline with 0.1% Tween-20; BP337–500, Fisher BioReagents, USA). Initial blocking was performed using 1-hr incubation with 3% normal donkey serum (NDS, 017–000-121, Jackson ImmunoResearch Laboratories, Inc., USA). After another round of washing with PBST, the slices were incubated with anti-VGAT antibody (diluted 1:200 in 3% NDS, AGT-005, Alomone Labs, Israel) at 4 ^{o}C overnight. The next day, brain tissues were rinsed with PBST and incubated with anti-rabbit Alexa Fluor 647 Donkey-secondary antibody (1:500, 711–605-152, Jackson ImmunoResearch Laboratories, Inc., USA) for 1 h. After washing with PBS, these slices were mounted on a slide glass with DAPI-containing mounting solution.

Data inclusion criteria

All the mice that had viral expression in the region of interest were included in the data. Mice that had no viral expression or misplaced optical fibers due to a mistake in surgery were excluded from the data.

Imaging

Images were taken with either an automatic fluorescence microscope (BZ-X710, Keyence) using included imaging software (BZ-X viewer, Keyence) or with a scanning confocal microscope (FV 1000, Olympus) using Fluoview software (Olympus). For quantification, images were processed with the same gain, offset, and exposure time. Cell counting for retrograde tracing was done manually.

Statistical analysis

All data are presented as mean ± S.E.M. The Shapiro-Wilk normality test was performed for choosing parametric/ nonparametric analysis. All one-factor experiments passed the normality test, and therefore the data were analyzed with parametric tests (Student's t-tests, repeated measures one-way ANOVAs with Sidak's post hoc comparison). Two-factor experiments were analyzed with repeated measures two-way ANOVAs for parametric or mixed-effects analysis (Mixed-effects model (REML) with fixed effects (type III)) for nonparametric tests with Sidak's post hoc comparison. Power analysis was performed with $\alpha = 0.05$ for confirming adequate n values in the experiments. Experiments were blinded to group allocation during behavioral data collection and analysis. Statistical analyses were performed using Prism 9 (GraphPad Software) and SigmaPlot 15.0 (Inpixion, USA). NS, $P>0.05$, * $P<0.05$, ** $P<0.01$, *** $P<0.001$. Full details of statistical tests in individual figures are described in the figure legend and Supplementary Table 3.

Extended Data

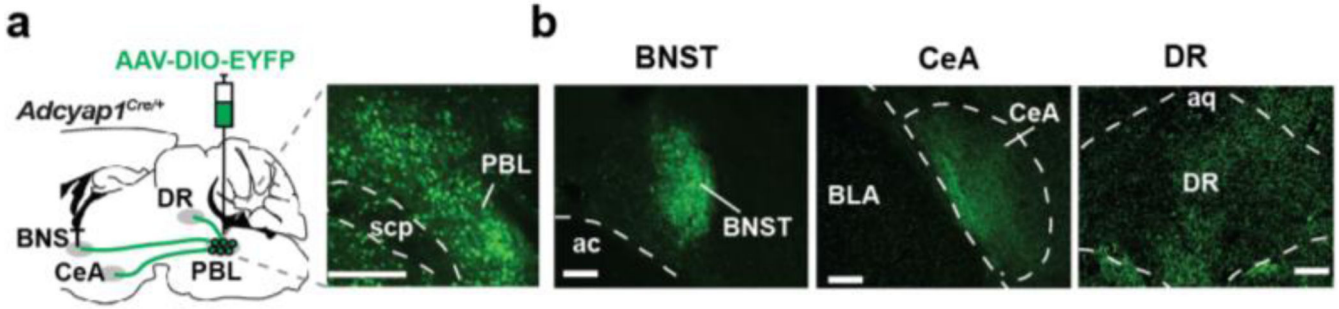

Extended Data 1. Projections from PACAP^{PBL} neurons.

a, Schematic and histological confirmation of Cre-dependent expression of EYFP in the PBL of an *Adcyap1*$^{Cre/+}$ mouse. Scale bars: 100 μm. **b**, Representative images of the output regions of PACAP^{PBL} neurons. Scale bars: 100 μm. Injections were repeated on three mice with similar results.

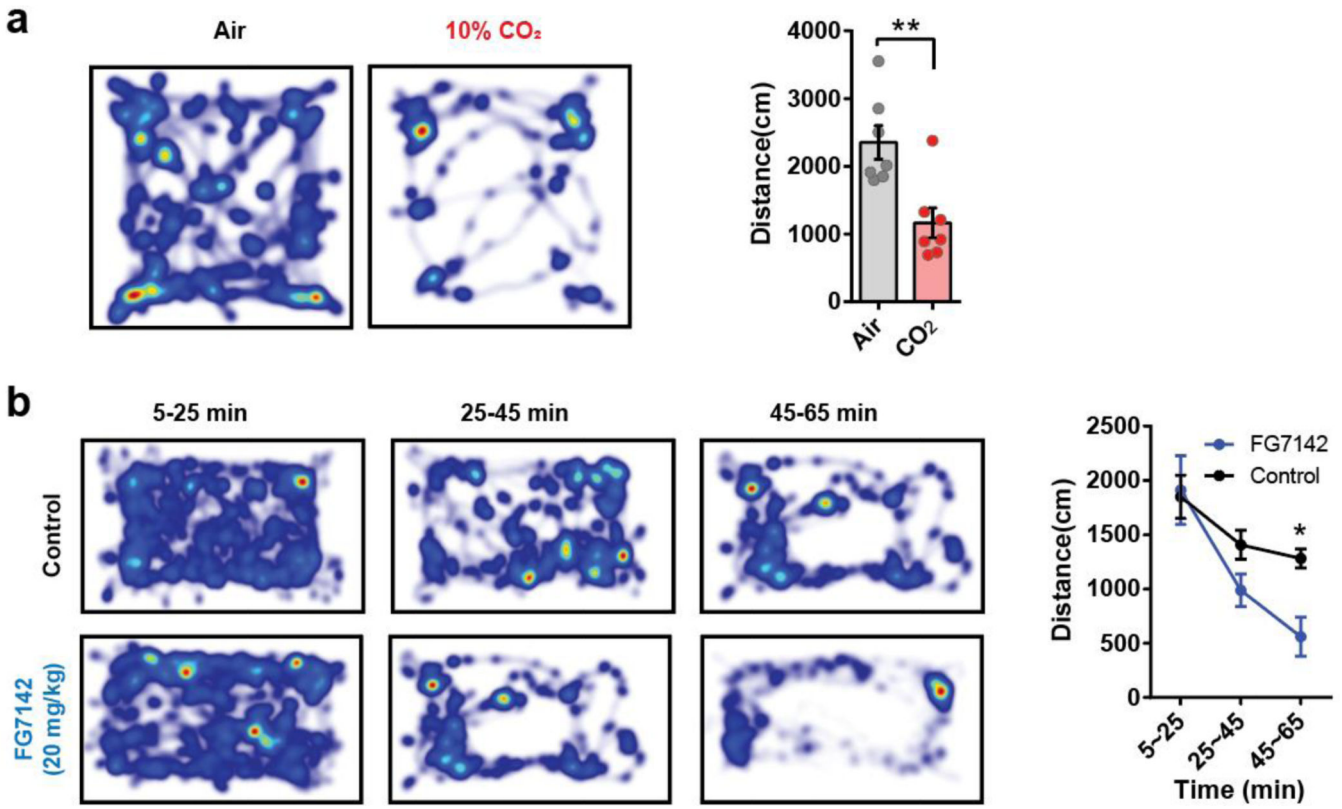

Extended Data 2. Behavioral changes of the PACAP$^{PBL\rightarrow DR}$::GCaMP6s mice during panicogenic conditions.

a, Heat map and distance traveled before- (normal air) and after CO_2 exposure. Paired two-sided *t*-test, $P < 0.001$. n = 7 mice. **b**, Heat map and distance traveled following FG-7142 or control injection. Repeated measure two-way ANOVA with Sidak's multiple comparisons test. n = 7 mice. Data are presented as the mean ± SEM; see also Supplementary Table 3 for statistical details. *P<0.05, **P<0.01.

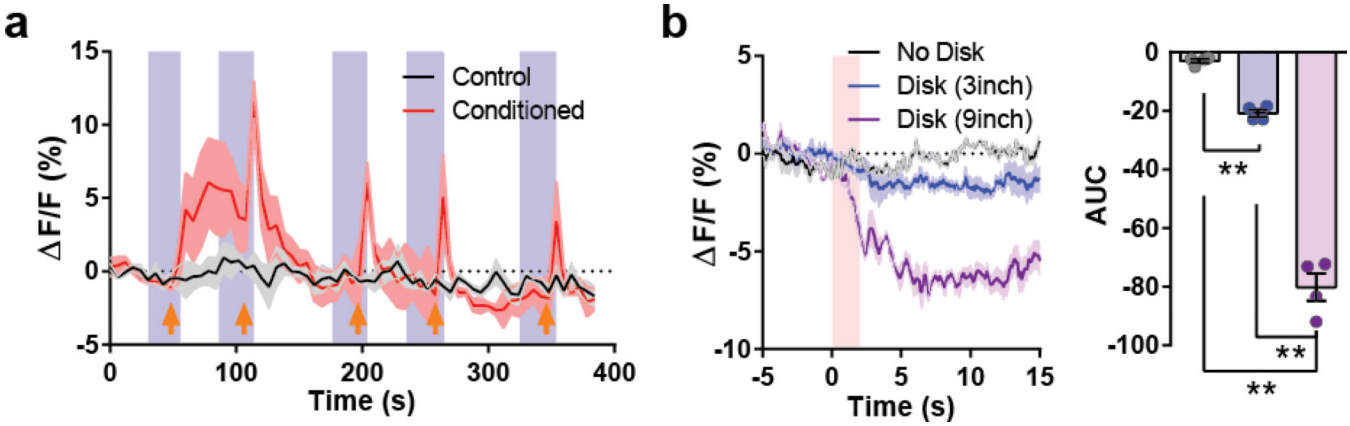

Extended Data 3. Calcium activity changes in PACAP$^{PBL\rightarrow DR}$ neurons do not respond as a general multi-modal aversive circuit.

a, Average calcium trace during "Conditioning" phase of the fear conditioning test. Blue shading indicates "Tone ON" periods and orange arrows indicate when the foot shock was

given. n = 3 mice. **b**, Average calcium trace during the looming test with corresponding AUC analysis. Pink shading indicates the 2-s looming exposure. Repeated measure one-way ANOVA with Sidak's multiple comparisons test, F (2, 6) = 240.127, $P < 0.001$. n = 4 mice. Data are presented as the mean ± SEM; see also Supplementary Table 3 for statistical details. ** $P<0.01$.

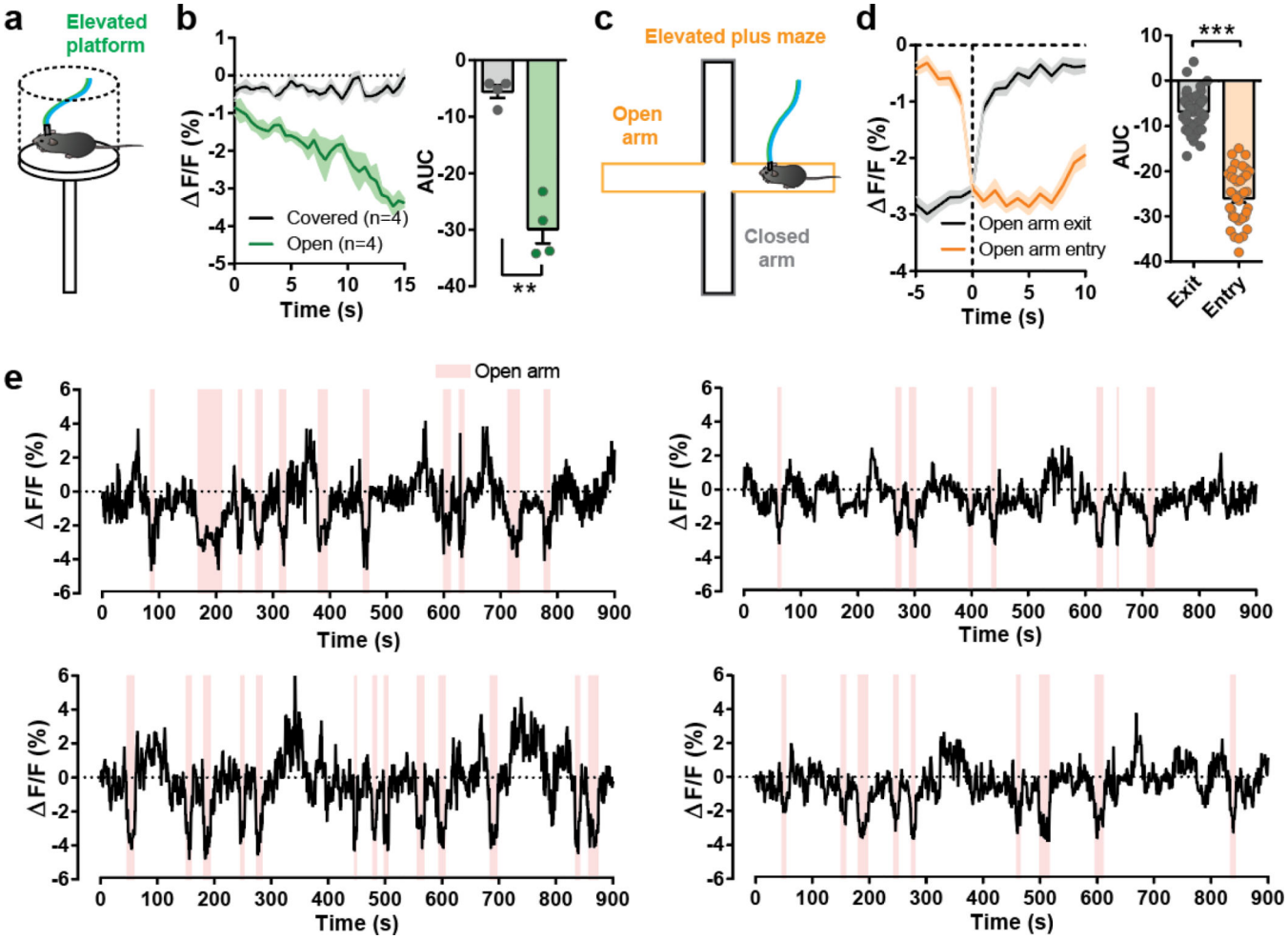

Extended Data 4. Calcium activity changes in PACAP$^{PBL\rightarrow DR}$ neurons during anxiogenic conditions.

a, Schematic of the elevated platform test. **b**, Average calcium trace during elevated platform assessment, and corresponding area under curve (AUC) analysis. Paired two-sided *t*-test, $P = 0.0017$. n = 4 mice. **c**, Schematic of the elevated plus maze. **d**, Average calcium trace during the seconds immediately preceding and following open arm entry and exit, with corresponding AUC analysis. Paired two-sided *t*-test, $P < 0.0001$. n = 4 mice. **e**, Calcium traces from individual animals. Pink shading indicates when mice were in the open arm. n = 4 mice. Data are presented as the mean ± SEM; see also Supplementary Table 3 for statistical details. ** $P<0.01$, *** $P<0.001$.

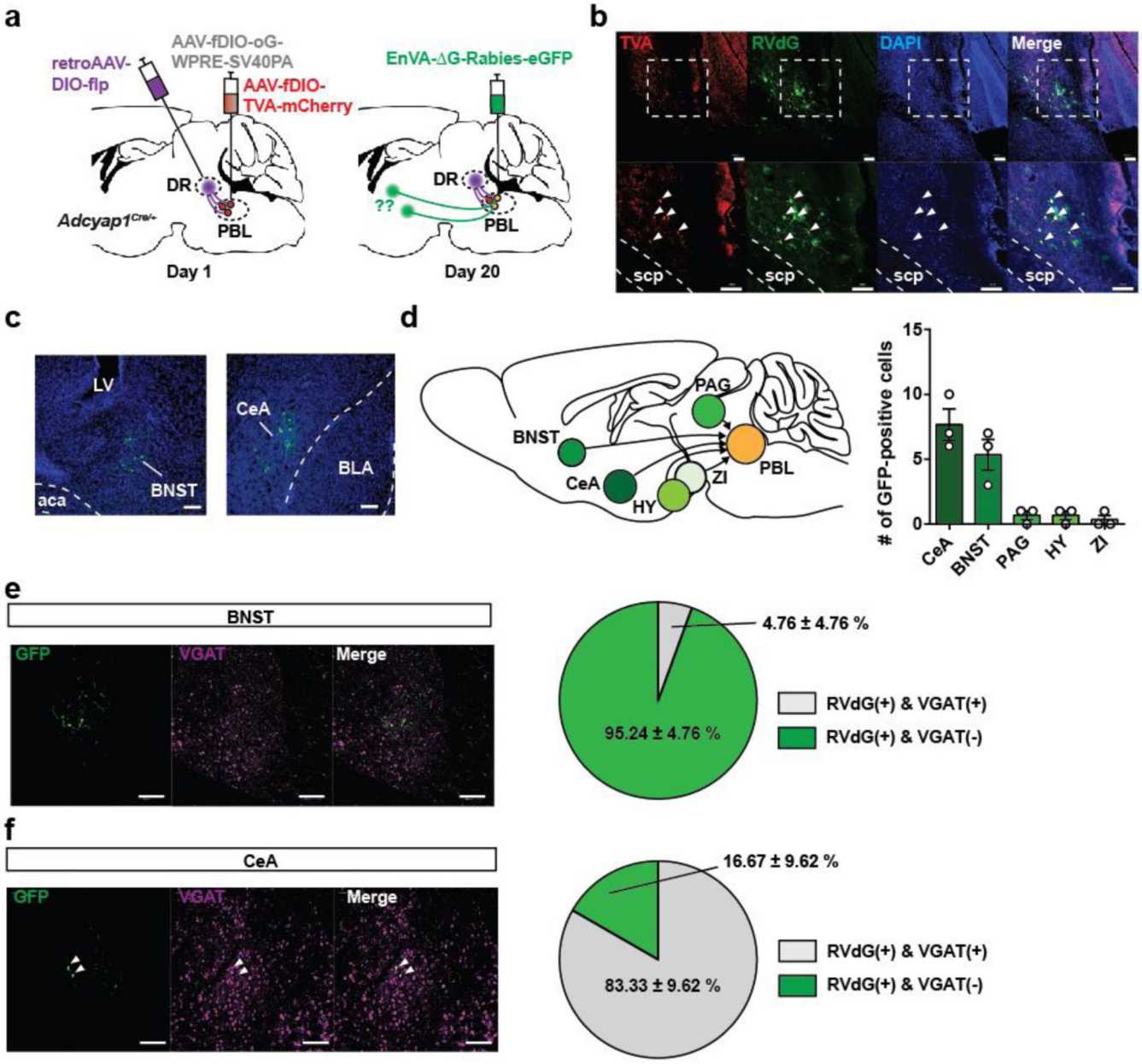

Extended Data 5. Inputs to PACAP$^{PBL\rightarrow DR}$ neurons.

a, Schematics of Cre- and Flp-dependent retrograde tracing in PBL of an *Adcyap1*$^{Cre/+}$ mouse for identification of inputs to PACAP$^{PBL\rightarrow DR}$ neurons. **b**, Histology of TVA and RVdG expression in PBL. Scale bars: 50 μm. Injections were repeated on three mice with similar results. **c**, Representative images of cTRIO tracing in BNST and CeA. Scale bars: 50 μm. Injections were repeated on three mice with similar results. **d**, Schematic of inputs to PACAP$^{PBL\rightarrow DR}$ neurons. Repeated measure one-way ANOVA with Sidak's multiple comparisons test, F (4, 8) = 21.871, P = 0.0073. n = 3 mice. **e**,**f**, Histological images of RVdG and VGAT expression, and graphical representation of the percentage of VGAT colocalization in BNST (e) and CeA (f). Scale bars: 50 μm. n = 3 mice. Data are presented as the mean ± SEM; see also Supplementary Table 3 for counting and statistical details.

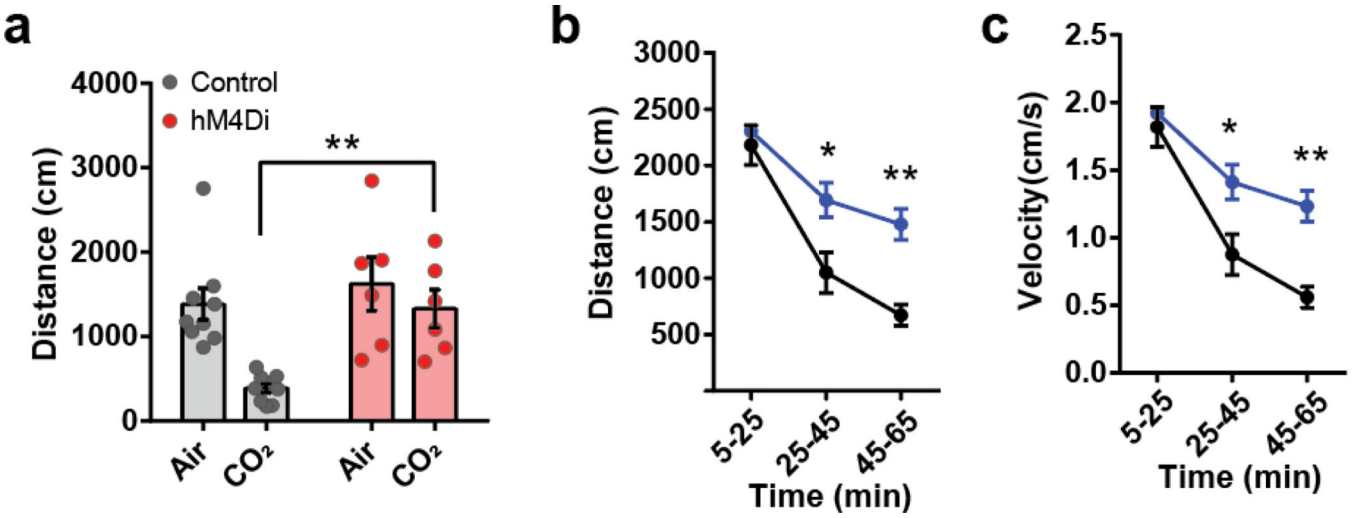

Extended Data 6. Inhibition of PACAP$^{PBL\rightarrow DR}$ neurons attenuates panic-like symptoms.

a, Distance traveled before (normal air) and after CO_2 exposure during chemogenetic inhibition of PACAP$^{PBL\rightarrow DR}$ neurons. Mixed-effects analysis with Sidak's multiple comparisons test. n = 9 control mice, n = 6 hM4Di mice. **b,c**, Distance traveled (b, repeated measures two-way ANOVA with Sidak's multiple comparisons test) and velocity (c, repeated measures two-way ANOVA with Sidak's multiple comparisons test) after FG-7142 injection during chemogenetic inhibition of PACAP$^{PBL\rightarrow DR}$ neurons. n = 9 control mice, n = 5 hM4Di mice. Data are presented as the mean ± SEM; see also Supplementary Table 3 for statistical details. *P<0.05, **P<0.01.

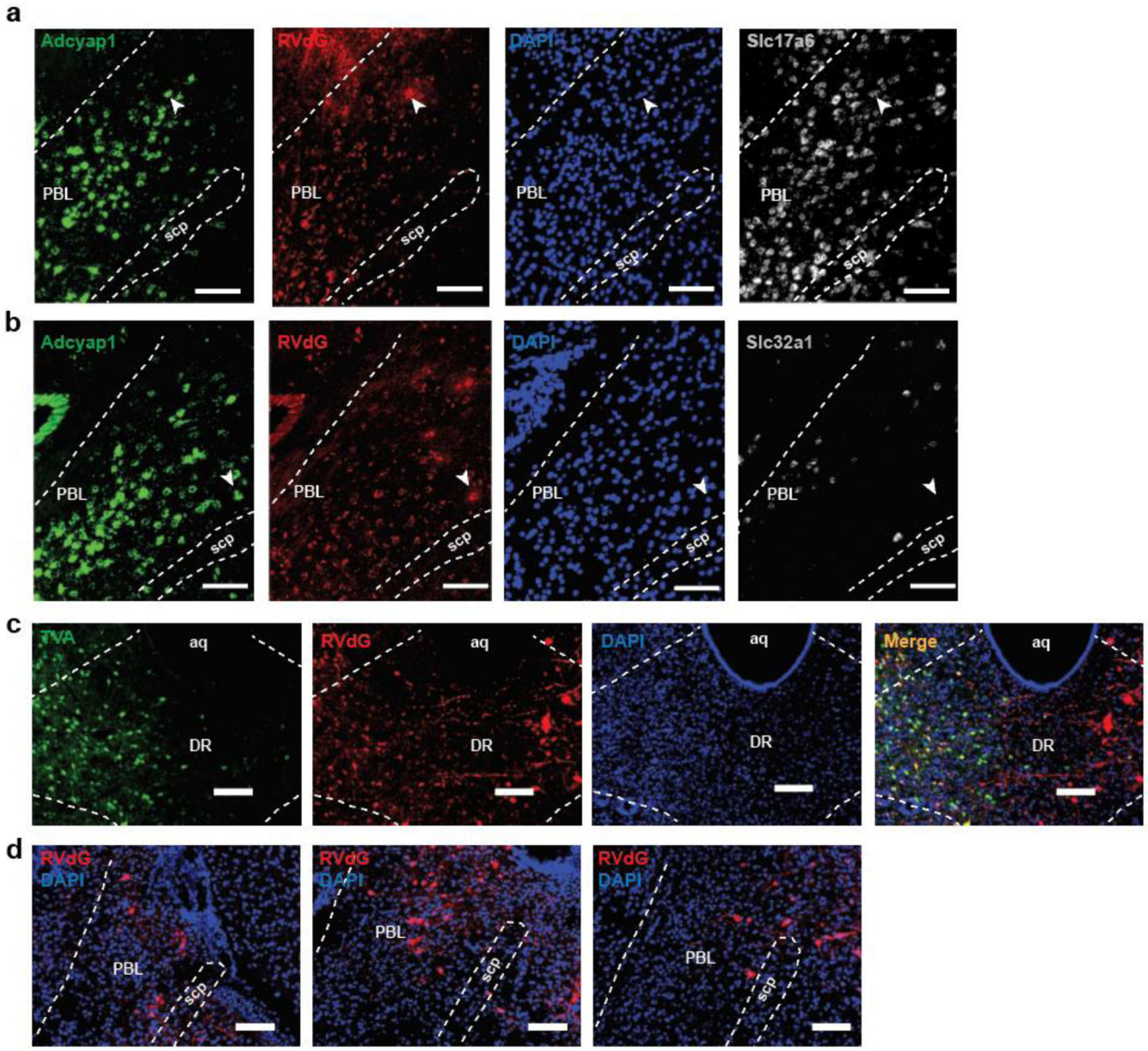

Extended Data 7. PAC1R^{DR} neurons are monosynaptically connected with PACAP^{PBL} neurons

a, Single channel histological images of Fig.7g. Presynaptic PACAP^{PBL} neurons are also VGluT2 (*Slc17a6*) positive. **b**, Single channel histological images of Fig.7h. Presynaptic PACAP^{PBL} neurons do not overlap with VGAT (*Slc32a1*). **c**, Histological images of DR after perfusing the retrograde rabies tracing mice. TVA (green), RVdG (red). Starter cells are observable. **d**, Representative images of presynaptic cells (RVdG, red) in PBL. Scale bars: 100 μm. This experiment was repeated on three mice with similar results.

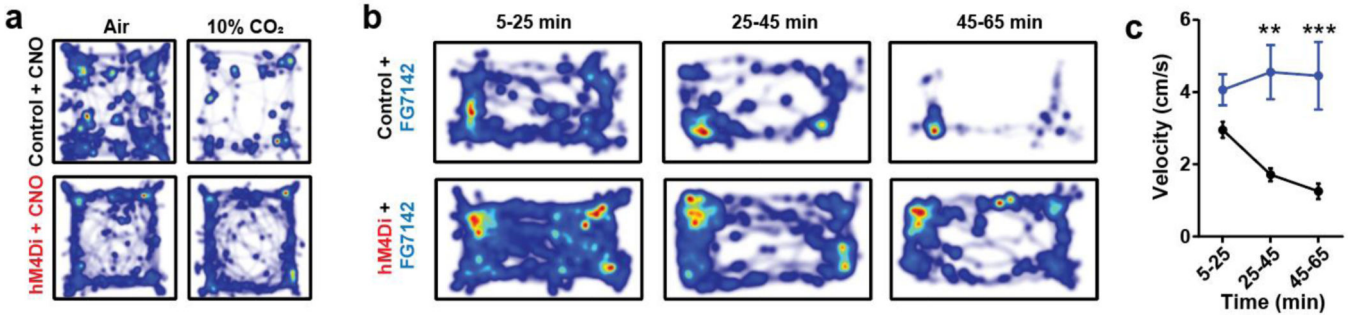

Extended Data 8. Inhibition of PAC1R^{DR} neurons blocks panic-like symptoms.
a, Heat map of mouse activity before (air) and after CO_2 exposure during chemogenetic inhibition of PAC1R^{DR} neurons. n = 7 mice per group. **b,c**, Heat map of mouse activity (b) and velocity (c, mixed-effects analysis with Sidak's multiple comparisons test and adjusted *P* values) after FG-7142 injection during chemogenetic inhibition of PAC1R^{DR} neurons. n = 7 mice per group. Data are presented as the mean ± SEM; see also Supplementary Table 3 for statistical details. ** $P<0.01$, *** $P<0.001$.

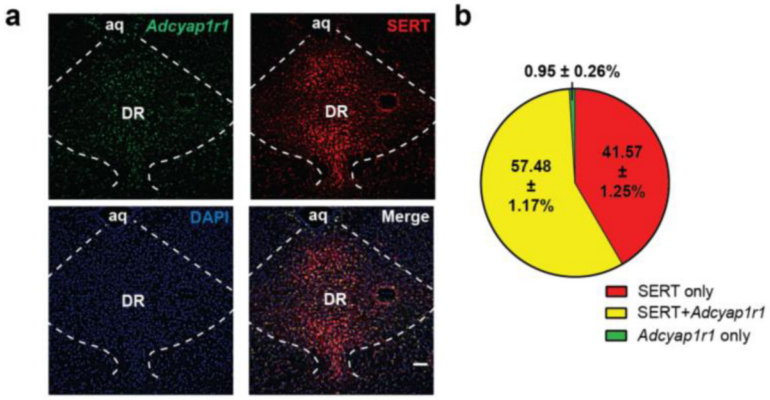

Extended Data 9. The majority of PAC1R (*Adcyap1r1*) neurons are SERT-positive.
a, Representative *in situ* hybridization images of PAC1R- (*Adcyap1r1*) and SERT-positive neurons in the DR (left). **b**, Graphical representation of percentages of fluorescent neurons. n = 7 mice. Scale bars: 50 μm. Data are presented as the mean ± SEM.; see also Supplementary Table 2 for counting details.

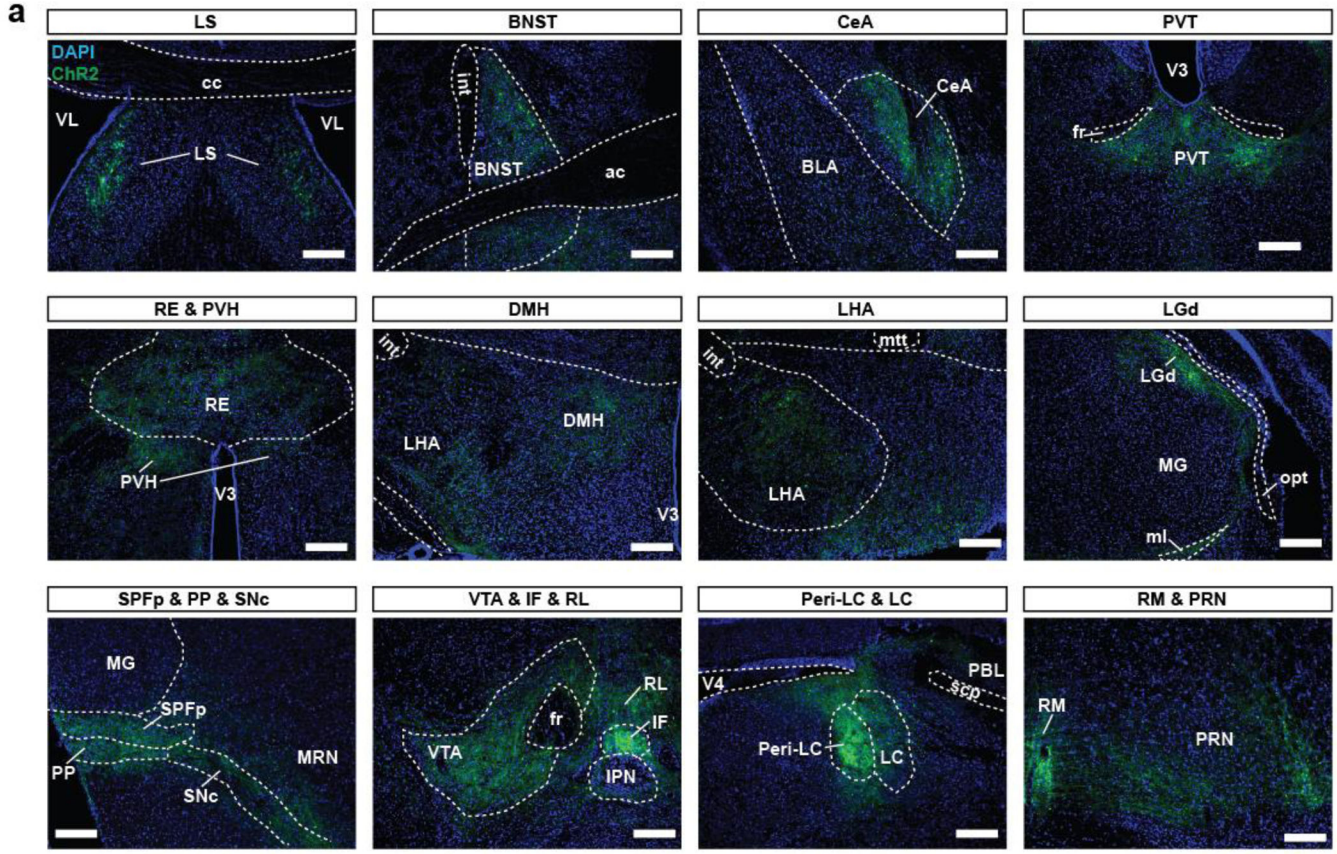

Extended Data 10. Projection targets of PAC1R^{DR} neurons.

a, Histological images of output regions from PAC1R^{DR} neurons expressing ChR2. Abbreviations: lateral septal nucleus (LS), BNST, CeA, paraventricular nucleus of the thalamus (PVT), nucleus of reuniens (RE), paraventricular hypothalamic nucleus (PVH), lateral hypothalamus (LHA), dorsomedial nucleus of the hypothalamus (DMH), lateral geniculate complex (LGd), subparafascicular nucleus parviceullar part (SPFp), peripeduncular nucleus (PP), substantia nigra compact part (SNc), ventral tegmental area (VTA), ifterfascicular nucleus raphe (IF), rostral linear uncleus raphe (RL), Peri-locus ceruleus (Peri-LC), LC, nucleus raphe magnus (RM), and pontine reticular nucleus (PRN). Scale bars: 100 μm. n = 5 mice.

Supplementary Material

Refer to Web version on PubMed Central for supplementary material.

Acknowledgments:

We thank members of the Han laboratory for the critical discussion of the paper and D. O'Keefe for critical input on the manuscript. We also thank Seahyung Park for proof-reading the response letter to the reviewers.

Funding:

National Institutes of Mental Health Biobehavioral Research Award for Innovative New Scientists (BRAINS) grant 1R01MH116203 (SH)

Bridge to Independence award from the Simons Foundation Autism Research Initiative SFARI #388708 (SH)

Data and materials availability:

All data associated with this study are available in the Source Code or the supplementary information.

REFERENCES

1. Killgore WDS et al. Cortico-Limbic Responses to Masked Affective Faces Across Ptsd, Panic Disorder, and Specific Phobia. Depression and Anxiety 31, 150–159 (2014). [PubMed: 23861215]
2. Crowe RR, Noyes R, Pauls DL & Slymen D. A family study of panic disorder. Archives of General Psychiatry 40, 1065–1069 (1983). [PubMed: 6625855]
3. Katon W. Panic disorder and somatization. Review of 55 cases. The American Journal of Medicine 77, 101–106 (1984). [PubMed: 6377887]
4. Meuret AE, Kroll J & Ritz T. Panic Disorder Comorbidity with Medical Conditions and Treatment Implications. Annu. Rev. Clin. Psychol. 13, 209–240 (2017). [PubMed: 28375724]
5. Gorman JM, Kent JM, Sullivan GM & Coplan JD. Neuroanatomical hypothesis of panic disorder, revised. The American Journal of Psychiatry 157, 493–505 (2000). [PubMed: 10739407]
6. Coplan JD & Lydiard RB. Brain circuits in panic disorder. Biological Psychiatry 44, 1264–1276 (1998). [PubMed: 9861469]
7. Shekhar A, Sajdyk TJ, Gehlert DR & Rainnie DG. The amygdala, panic disorder, and cardiovascular responses. Annals of the New York Academy of Sciences 985, 308–325 (2003). [PubMed: 12724167]
8. Kim JE, Dager SR & Lyoo IK. The role of the amygdala in the pathophysiology of panic disorder: evidence from neuroimaging studies. Biology of Mood & Anxiety Disorders 2, 20 (2012). [PubMed: 23168129]
9. Yoon S et al. Subregional Shape Alterations in the Amygdala in Patients with Panic Disorder. PLoS ONE 11, e0157856 (2016).
10. Feinstein JS, Adolphs R, Damasio A & Tranel D. The human amygdala and the induction and experience of fear. Current biology: CB 21, 34–38 (2011). [PubMed: 21167712]
11. Khalsa SS et al. Panic Anxiety in Humans with Bilateral Amygdala Lesions: Pharmacological Induction via Cardiorespiratory Interoceptive Pathways. The Journal of Neuroscience: The Official Journal of the Society for Neuroscience 36, 3559–3566 (2016). [PubMed: 27013684]
12. Feinstein JS et al. Fear and panic in humans with bilateral amygdala damage. Nature neuroscience 16, 270–272 (2013). [PubMed: 23377128]
13. Chiang MC et al. Parabrachial Complex: A Hub for Pain and Aversion. Journal of Neuroscience 39, 8225–8230 (2019). [PubMed: 31619491]
14. Han S, Soleiman MT, Soden ME, Zweifel LS & Palmiter RD. Elucidating an Affective Pain Circuit that Creates a Threat Memory. Cell 162, 363–374 (2015). [PubMed: 26186190]
15. Davern PJ. A role for the lateral parabrachial nucleus in cardiovascular function and fluid homeostasis. Frontiers in Physiology 5, 436 (2014). [PubMed: 25477821]
16. Yahiro T, Kataoka N, Nakamura Y & Nakamura K. The lateral parabrachial nucleus, but not the thalamus, mediates thermosensory pathways for behavioural thermoregulation. Scientific Reports 7, 5031 (2017). [PubMed: 28694517]
17. Liu S et al. Neural basis of opioid-induced respiratory depression and its rescue. Proceedings of the National Academy of Sciences 118, (2021).
18. Bourin M, Baker GB & Bradwejn J. Neurobiology of panic disorder. Journal of Psychosomatic Research 44, 163–180 (1998). [PubMed: 9483472]
19. Singewald N & Sharp T. Neuroanatomical targets of anxiogenic drugs in the hindbrain as revealed by Fos immunocytochemistry. Neuroscience 98, 759–770 (2000). [PubMed: 10891619]
20. Brannan S et al. Neuroimaging of cerebral activations and deactivations associated with hypercapnia and hunger for air. PNAS 98, 2029–2034 (2001). [PubMed: 11172070]

21. Perna G, Caldirola D & Bellodi L. Panic disorder: from respiration to the homeostatic brain. Acta Neuropsychiatrica 16, 57–67 (2004). [PubMed: 26983998]
22. Cardoso JCR, Garcia MG & Power DM. Tracing the Origins of the Pituitary Adenylate-Cyclase Activating Polypeptide (PACAP). Frontiers in Neuroscience 14, 366 (2020). [PubMed: 32508559]
23. Zhang L et al. Behavioral role of PACAP signaling reflects its selective distribution in glutamatergic and GABAergic neuronal subpopulations. eLife 10, e61718 (2021). [PubMed: 33463524]
24. Stroth N, Holighaus Y, Ait-Ali D & Eiden LE. PACAP: a master regulator of neuroendocrine stress circuits and the cellular stress response. Annals of the New York Academy of Sciences 1220, 49–59 (2011). [PubMed: 21388403]
25. Ressler KJ et al. Post-traumatic stress disorder is associated with PACAP and the PAC1 receptor. Nature 470, 492–497 (2011). [PubMed: 21350482]
26. Cho J-H et al. Pituitary Adenylate Cyclase-Activating Polypeptide Induces Postsynaptically Expressed Potentiation in the Intra-amygdala Circuit. J. Neurosci. 32, 14165–14177 (2012). [PubMed: 23055486]
27. Iurato S et al. “DNA Methylation signatures in panic disorder”. Translational Psychiatry 7, 1–10 (2017).
28. Erhardt A, Lucae S, Ising M, Holsboer F & Binder EB. Association of PACAP and PACAPR1 gene variants with unipolar depression and panic disorder. Pharmacopsychiatry 46, A89 (2013).
29. Evans AK & Lowry CA. Pharmacology of the β-Carboline FG-7142, a Partial Inverse Agonist at the Benzodiazepine Allosteric Site of the GABAA Receptor: Neurochemical, Neurophysiological, and Behavioral Effects. CNS Drug Reviews 13, 475–501 (2007). [PubMed: 18078430]
30. Ye J & Veinante P. Cell-type specific parallel circuits in the bed nucleus of the stria terminalis and the central nucleus of the amygdala of the mouse. Brain Structure and Function 224, 1067–1095 (2019). [PubMed: 30610368]
31. Boucher MN, Aktar M, Braas KM, May V & Hammack SE. Activation of Lateral Parabrachial Nucleus (LPBn) PACAP-Expressing Projection Neurons to the Bed Nucleus of the Stria Terminalis (BNST) Enhances Anxiety-like Behavior. J Mol Neurosci (2021) doi:10.1007/s12031-021-01946-z.
32. Missig G et al. Parabrachial nucleus (PBn) pituitary adenylate cyclase activating polypeptide (PACAP) signaling in the amygdala: implication for the sensory and behavioral effects of pain. Neuropharmacology 86, 38–48 (2014). [PubMed: 24998751]
33. Ziemann AE et al. The Amygdala is a Chemosensor that Detects Carbon Dioxide and Acidosis to Elicit Fear Behavior. Cell 139, 1012–1021 (2009). [PubMed: 19945383]
34. Leibold NK et al. CO2 exposure as translational cross-species experimental model for panic. Translational Psychiatry 6, e885–e885 (2016). [PubMed: 27598969]
35. Perna G et al. Carbon dioxide/oxygen challenge test in panic disorder. Psychiatry Research 52, 159–171 (1994). [PubMed: 7972572]
36. Dorow R, Horowski R, Paschelke G, Amin M & Braestrup C. SEVERE ANXIETY INDUCED BY FG 7142, A β-CARBOLINE LIGAND FOR BENZODIAZEPINE RECEPTORS. The Lancet 322, 98–99 (1983).
37. McGregor IS, Lee AM & Westbrook RF. Stress-induced changes in respiratory quotient, energy expenditure and locomotor activity in rats: effects of midazolam. Psychopharmacology 116, 475–482 (1994). [PubMed: 7701052]
38. Patki G et al. Tempol Treatment Reduces Anxiety-Like Behaviors Induced by Multiple Anxiogenic Drugs in Rats. PLOS ONE 10, e0117498 (20 2015).
39. Federici LM, Caliman IF, Fitz SD, Shekhar A & Johnson PL. Select panicogenic drugs and stimuli induce consistent increases in tail skin flushes and decreases in core body temperature. Behavioural Pharmacology 30, 376–382 (2019). [PubMed: 30480550]
40. Salchner P et al. Airjet and FG-7142-induced Fos expression differs in rats selectively bred for high and low anxiety-related behavior. Neuropharmacology 50, 1048–1058 (2006). [PubMed: 16620881]
41. Johnson PL et al. Orexin 1 receptors are a novel target to modulate panic responses and the panic brain network. Physiology & Behavior 107, 733–742 (2012). [PubMed: 22554617]

42. Palmiter RD. The Parabrachial Nucleus: CGRP Neurons Function as a General Alarm. Trends in Neurosciences 41, 280–293 (2018). [PubMed: 29703377]
43. Kang SJ et al. A central alarm system that gates multi-sensory innate threat cues to the amygdala. Cell Reports 40, 111222 (2022). [PubMed: 35977501]
44. Iversen SD. 5-HT and anxiety. Neuropharmacology 23, 1553–1560 (1984). [PubMed: 6152028]
45. Kahn RS, Asnis GM, Wetzler S & Praag HM. Neuroendocrine evidence for serotonin receptor hypersensitivity in panic disorder. Psychopharmacology 96, 360–364 (1988). [PubMed: 2906153]
46. Kahn RS, Wetzler S, Praag HM, Asnis GM & Strauman T. Behavioral indications for serotonin receptor hypersensitivity in panic disorder. Psychiatry Research 25, 101–104 (1988). [PubMed: 3217461]
47. Ren J et al. Anatomically Defined and Functionally Distinct Dorsal Raphe Serotonin Sub-systems. Cell 175, 472–487.e20 (2018). [PubMed: 30146164]
48. Paul ED & Lowry CA. Functional topography of serotonergic systems supports the Deakin/Graeff hypothesis of anxiety and affective disorders. Journal of Psychopharmacology (Oxford, England) 27, 1090–1106 (2013). [PubMed: 23704363]
49. Luskin AT et al. A diverse network of pericoerulear neurons control arousal states. bioRxiv 2022.06.30.498327 (2022) doi:10.1101/2022.06.30.498327.
50. Borkar CD et al. Sex differences in behavioral responses during a conditioned flight paradigm. Behavioural Brain Research 389, 112623 (2020).
51. Dorofeikova M et al. Effects of footshock stress on social behavior and neuronal activation in the medial prefrontal cortex and amygdala of male and female mice. PLOS ONE 18, e0281388 (2023).
52. Eiden LE, Goosens KA, Jacobson KA, Leggio L & Zhang L. Peptide-Liganded G Protein-Coupled Receptors as Neurotherapeutics. ACS Pharmacol. Transl. Sci. 3, 190–202 (2020). [PubMed: 32296762]
53. Spampanato J, Polepalli J & Sah P. Interneurons in the basolateral amygdala. Neuropharmacology 60, 765–773 (2011). [PubMed: 21093462]
54. Gilpin NW, Herman MA & Roberto M. The Central Amygdala as an Integrative Hub for Anxiety and Alcohol Use Disorders. Biological psychiatry 77, 859–869 (2015). [PubMed: 25433901]
55. Duvarci S, Popa D & Paré D. Central Amygdala Activity during Fear Conditioning. The Journal of Neuroscience 31, 289–294 (2011). [PubMed: 21209214]
56. Fogaça MV & Duman RS. Cortical GABAergic Dysfunction in Stress and Depression: New Insights for Therapeutic Interventions. Frontiers in Cellular Neuroscience 13, (2019).
57. Brambilla P, Perez J, Barale F, Schettini G & Soares JC. GABAergic dysfunction in mood disorders. Molecular Psychiatry 8, 721–737 (2003). [PubMed: 12888801]
58. Maller RG & Reiss S. Anxiety sensitivity in 1984 and panic attacks in 1987. Journal of Anxiety Disorders 6, 241–247 (1992).
59. Goodwin RD et al. Panic Attack as a Risk Factor for Severe Psychopathology. American Journal of Psychiatry 161, 2207–2214 (2004). [PubMed: 15569891]
60. Coryell W et al. Depression and panic attacks: the significance of overlap as reflected in follow-up and family study data. The American Journal of Psychiatry 145, 293–300 (1988). [PubMed: 3344844]
61. Walker DL, Toufexis DJ & Davis M. Role of the bed nucleus of the stria terminalis versus the amygdala in fear, stress, and anxiety. European Journal of Pharmacology 463, 199–216 (2003). [PubMed: 12600711]
62. Lee Y & Davis M. Role of the Hippocampus, the Bed Nucleus of the Stria Terminalis, and the Amygdala in the Excitatory Effect of Corticotropin-Releasing Hormone on the Acoustic Startle Reflex. J. Neurosci. 17, 6434–6446 (1997). [PubMed: 9236251]
63. Waddell J, Morris RW & Bouton ME. Effects of bed nucleus of the stria terminalis lesions on conditioned anxiety: Aversive conditioning with long-duration conditional stimuli and reinstatement of extinguished fear. Behavioral Neuroscience 120, 324–336 (2006). [PubMed: 16719697]

64. Taugher RJ et al. The Bed Nucleus of the Stria Terminalis Is Critical for Anxiety-Related Behavior Evoked by CO2 and Acidosis. Journal of Neuroscience 34, 10247–10255 (2014). [PubMed: 25080586]
65. Kaur S & Saper CB. Neural Circuitry Underlying Waking Up to Hypercapnia. Frontiers in Neuroscience 13, (2019).
66. Song G & Poon C-S. Lateral parabrachial nucleus mediates shortening of expiration and increase of inspiratory drive during hypercapnia. Respiratory physiology & neurobiology 165, 9–12 (2009). [PubMed: 18996229]
67. Breier A, Charney DS & Heninger GR. Agoraphobia With Panic Attacks: Development, Diagnostic Stability, and Course of Illness. Arch Gen Psychiatry 43, 1029–1036 (1986). [PubMed: 3767595]
68. Kessler RC et al. The Epidemiology of Panic Attacks, Panic Disorder, and Agoraphobia in the National Comorbidity Survey Replication. Arch Gen Psychiatry 63, 415–424 (2006). [PubMed: 16585471]
69. Chiang MC et al. Divergent Neural Pathways Emanating from the Lateral Parabrachial Nucleus Mediate Distinct Components of the Pain Response. Neuron 106, 927–939.e5 (2020). [PubMed: 32289251]
70. Sun L et al. Parabrachial nucleus circuit governs neuropathic pain-like behavior. Nature Communications 11, 5974 (2020).
71. Deakin JF & Graeff FG. 5-HT and mechanisms of defence. Journal of Psychopharmacology (Oxford, England) 5, 305–315 (1991). [PubMed: 22282829]
72. Graeff FG. Serotonin, the periaqueductal gray and panic. Neuroscience & Biobehavioral Reviews 28, 239–259 (2004). [PubMed: 15225969]
73. Pobbe RLH, Zangrossi H, Blanchard DC & Blanchard RJ. Involvement of dorsal raphe nucleus and dorsal periaqueductal gray 5-HT receptors in the modulation of mouse defensive behaviors. European Neuropsychopharmacology 21, 306–315 (2011). [PubMed: 20570114]
74. Bago M & Dean C. Sympathoinhibition from ventrolateral periaqueductal gray mediated by 5-HT1A receptors in the RVLM. American Journal of Physiology-Regulatory, Integrative and Comparative Physiology 280, R976–R984 (2001). [PubMed: 11247817]
75. Teissier A et al. Activity of Raphé Serotonergic Neurons Controls Emotional Behaviors. Cell Reports 13, 1965–1976 (2015). [PubMed: 26655908]
76. Correia PA et al. Transient inhibition and long-term facilitation of locomotion by phasic optogenetic activation of serotonin neurons. eLife 6, e20975 (2017). [PubMed: 28193320]
77. Seo C et al. Intense threat switches dorsal raphe serotonin neurons to a paradoxical operational mode. Science (2019).
78. Walsh JJ et al. 5-HT release in nucleus accumbens rescues social deficits in mouse autism model. Nature 560, 589–594 (2018). [PubMed: 30089910]
79. Cathala A et al. Serotonin2B receptor blockade in the rat dorsal raphe nucleus suppresses cocaine-induced hyperlocomotion through an opposite control of mesocortical and mesoaccumbens dopamine pathways. Neuropharmacology 180, 108309 (2020).
80. Kusljic S & Buuse MVD. Differential role of serotonin projections from the dorsal and median raphe nuclei in phencyclidine-induced hyperlocomotion and fos-like immunoreactivity in rats. Synapse 66, 885–892 (2012). [PubMed: 22733588]
81. Sukamoto T, Yamamoto T, Watanabe S & Ueki S. Cardiovascular responses to centrally administered serotonin in conscious normotensive and spontaneously hypertensive rats. European Journal of Pharmacology 100, 173–179 (1984). [PubMed: 6734715]
82. Gradin K, Qadri F, Nomikos GG, Hillegaart V & Svensson TH. Substance P injection into the dorsal raphe increases blood pressure and serotonin release in hippocampus of conscious rats. European Journal of Pharmacology 218, 363–367 (1992). [PubMed: 1385170]
83. Lovick TA. Influence of the dorsal and median raphe nuclei on neurons in the periaqueductal gray matter: Role of 5-hydroxytryptamine. Neuroscience 59, 993–1000 (1994). [PubMed: 8058131]
84. Courtney NA & Ford CP. Mechanisms of 5-HT1A receptor-mediated transmission in dorsal raphe serotonin neurons. The Journal of Physiology 594, 953–965 (2016). [PubMed: 26634643]

85. Gantz SC, Levitt ES, Llamosas N, Neve KA & Williams JT. Depression of Serotonin Synaptic Transmission by the Dopamine Precursor L-DOPA. Cell Reports 12, 944–954 (2015). [PubMed: 26235617]

86. Perna G, Schruers K, Alciati A & Caldirola D. Novel investigational therapeutics for panic disorder. Expert Opinion on Investigational Drugs 24, 491–505 (2015). [PubMed: 25539284]

87. Kaur S et al. Role of serotonergic dorsal raphe neurons in hypercapnia-induced arousals. Nature Communications 11, 2769 (2020).

Methods-only references

88. Cho H-Y, Kim M & Han J-H. Specific disruption of contextual memory recall by sparse additional activity in the dentate gyrus. Neurobiology of Learning and Memory 145, 190–198 (2017). [PubMed: 29031808]

89. Jeong Y et al. Synaptic plasticity-dependent competition rule influences memory formation. Nature Communications 12, 3915 (2021).

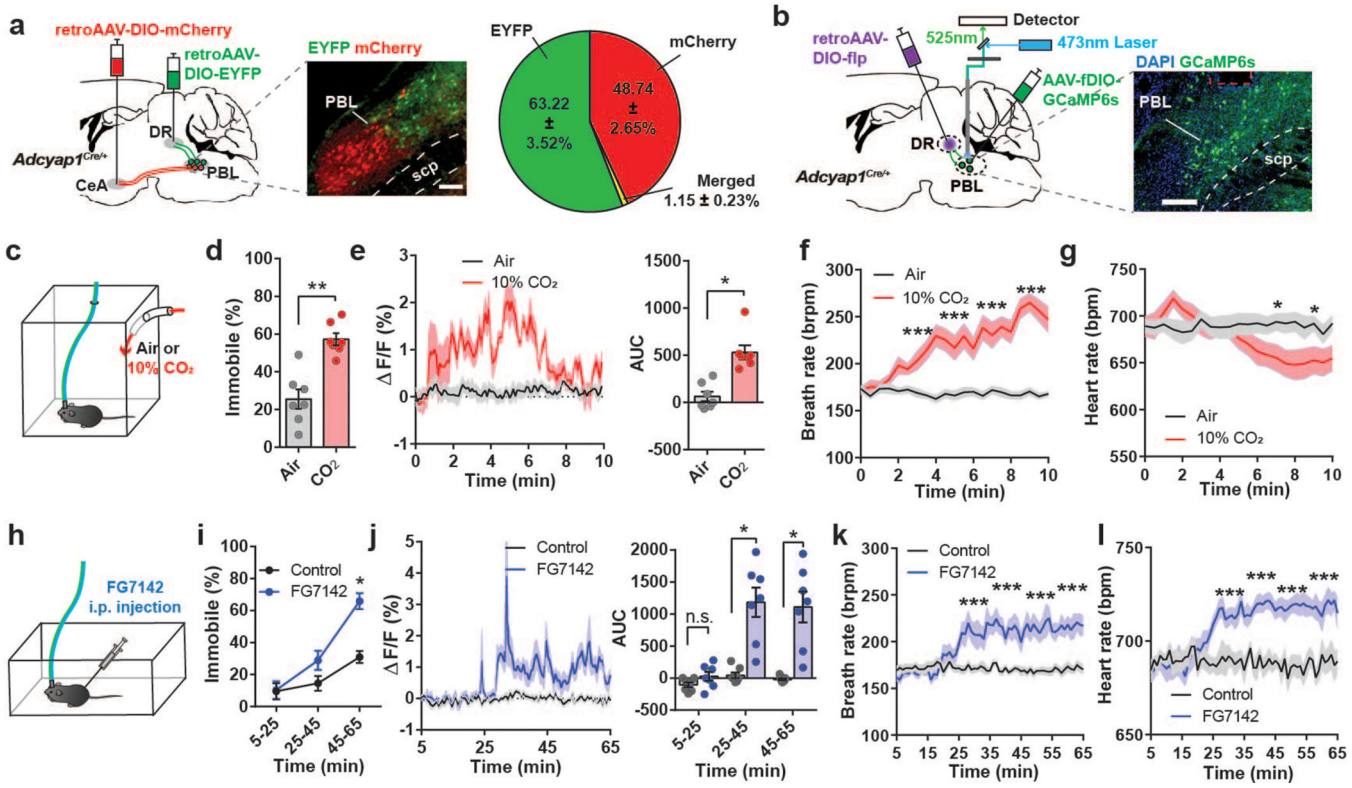

Fig. 1. Activity of PACAP$^{PBL→DR}$ neurons increases in panicogenic conditions.

a, Schematic and representative image of Cre-dependent retrograde expression of mCherry in PACAP^{PBL} neurons projecting to the CeA, and EYFP expression in DR-projecting PACAP^{PBL} neurons. Percentages of indicated fluorescent cells in the PBL are represented via a pie chart. Scale bar: 100 μm. Injections were repeated in 3 mice with similar results. **b**, Schematic and representative images of Cre- and Flp-dependent expression of GCaMP6s, as well as the implantation of fiber in the PBL of an *Adcyap1*$^{Cre/+}$ mouse to monitor PACAP$^{PBL→DR}$ neuronal activity via fiber photometry. Scale bar: 100 μm. This experiment was repeated on seven mice with similar results. **c**, Schematic of the CO_2 exposure test. **d**, Immobile behavior during 10 min of normal air (control condition) or 10% CO_2 exposure. Paired two-sided *t*-test, $P < 0.001$. n = 7 mice. **e**, Change in calcium activity during 10 min of air or 10% CO_2 exposure and corresponding AUC analysis. Paired two-sided *t*-test, $P = 0.0039$. n = 7 mice. **f**, **g**, Breathing (f, repeated measure two-way ANOVA with Sidak's multiple comparisons test), and heart rate (g, mixed-effects analysis with Sidak's multiple comparisons test) changes during CO_2 exposure. n = 14 mice. Respiration responses to both air and CO_2 exposure were taken from the same mice. Lines represent mean responses during each condition in the same mice. **h**, Schematic of FG-7142 (20 mg/kg) i.p. injection. **i**, Immobile behavior change following FG-7142 injection. Repeated measure two-way ANOVA with Sidak's multiple comparisons test. n = 7 mice. Time = 0 is when FG-7142 was injected and recordings started 5 mins after the injection. **j**, Change in calcium activity following i.p. injection of FG-7142, and corresponding AUC analysis within each 20-min bin. Repeated measure two-way ANOVA with Sidak's multiple comparisons test. n = 7 mice. **k**, **l**, Breathing (k, repeated measure two-way ANOVA with

Sidak’s multiple comparisons test), and heart rate (l, repeated measure two-way ANOVA with Sidak’s multiple comparisons test) changes 30 min after FG-7142 injection. n = 9 mice. Data are presented as the mean ± SEM; see also Supplementary Table 3 for statistical details. *P<0.05, **P<0.01, ***P<0.001.

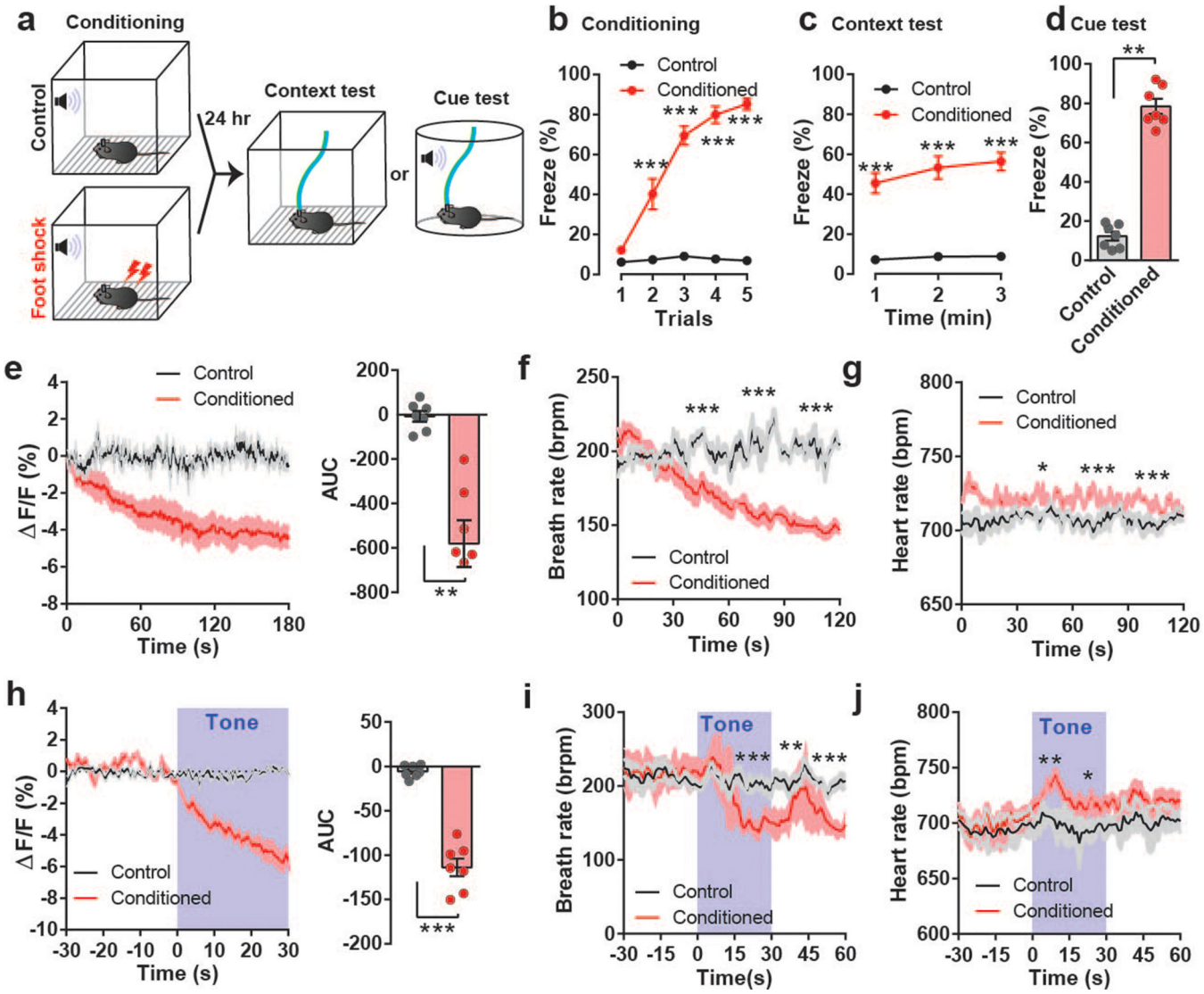

Fig. 2. Activity of PACAP$^{PBL\rightarrow DR}$ neurons decreases during retrieval in the fear conditioning test.

a, Schematic of the fear conditioning experiment. **b**–**d**, Freezing behavior during conditioning (b, repeated measure two-way ANOVA with Sidak's multiple comparisons test), context (c, repeated measure two-way ANOVA with Sidak's multiple comparisons test), and cue tests (d, paired two-sided *t*-test, $P < 0.001$). n = 7 mice. **e**, PACAP$^{PBL\rightarrow DR}$ calcium activity change during context test and corresponding AUC analysis. Paired two-sided *t*-test, $P = 0.0017$. n = 4 mice. **f**,**g**, Breathing (f, repeated measure two-way ANOVA with Sidak's multiple comparisons test), and heart rate (g, mixed-effects analysis with Sidak's multiple comparisons test) changes during the context test. n = 6 (control), n = 5 mice (conditioned). **h**, Calcium activity change during cue test and corresponding AUC during tone presentation. Paired two-sided *t*-test, $P < 0.001$. n = 7 mice. Tone presentation is denoted by blue shading. **i**,**j**, Breathing (i, repeated measure two-way ANOVA with Sidak's multiple comparisons test), and heart rate (j, repeated measure two-way ANOVA with Sidak's multiple comparisons test) changes during the cue test. n = 6 control mice, n =

5 conditioned mice. Data are presented as the mean ± SEM; see also Supplementary Table 3 for statistical details. *P<0.05, **P<0.01, ***P<0.001.

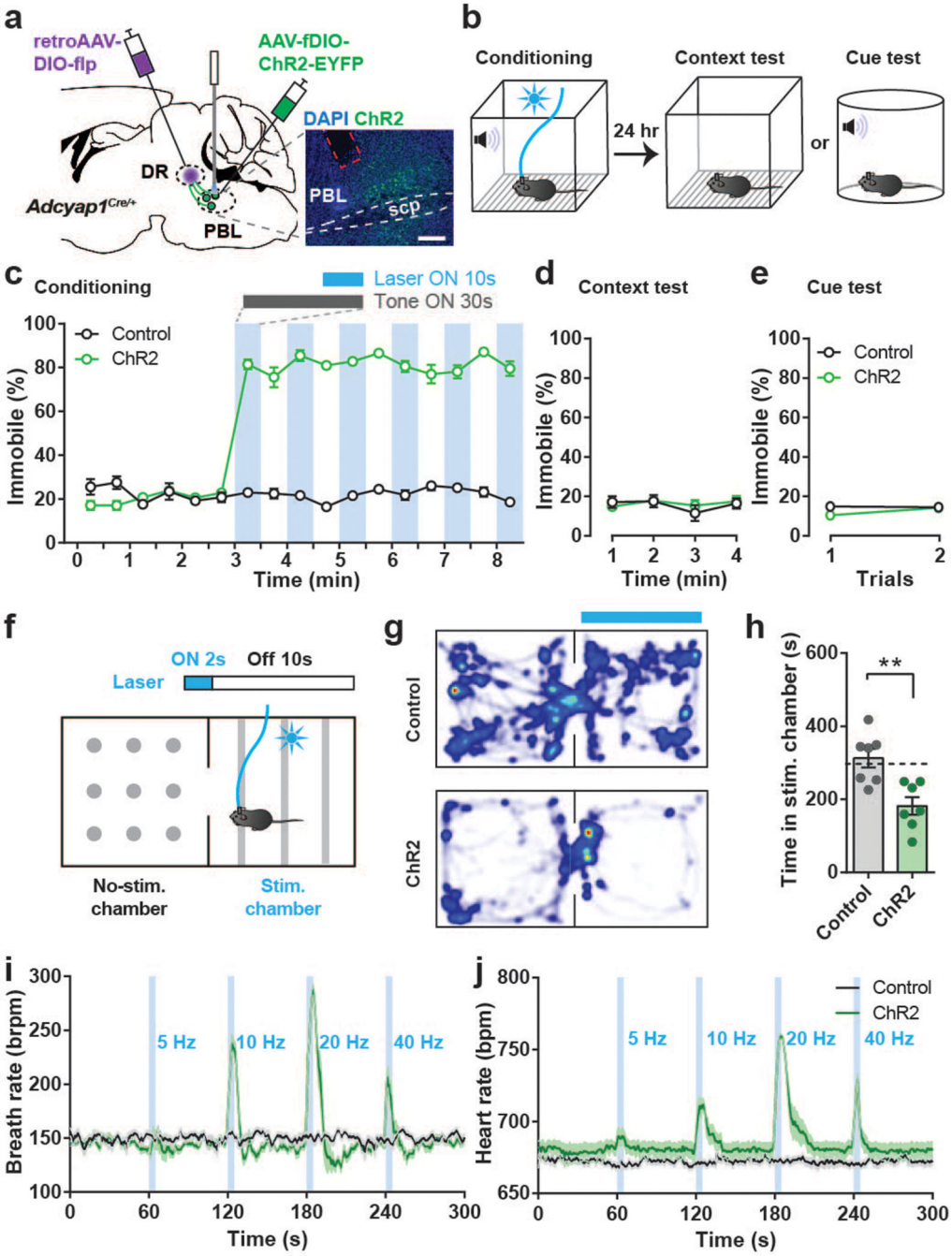

Fig. 3. Activation of PACAP$^{PBL\rightarrow DR}$ neurons produces panic-like symptoms without forming associative memory.

a, Schematic and histological confirmation of Cre- and Flp-dependent expression of ChR2 in the PBL of an *Adcyap1*$^{Cre/+}$ mouse for optogenetic activation of PACAP$^{PBL\rightarrow DR}$ neurons. Scale bars: 100 μm. This experiment was repeated on seven mice with similar results. **b**, Schematic of the optical conditioning test. **c**–**e** Immobility levels during conditioning (c), context (d), and cue assessments (e). n = 7 mice per group. Laser activation is denoted by blue shading. **f**, Schematic of the real-time place aversion test. **g**,**h**, Representative heat

maps of mouse activity (g), and average time spent in the stimulation-paired and non-paired chambers (h, unpaired two-sided *t*-test, $P = 0.003$). n = 7 mice per group. **i**,**j**, Breathing (i) and heart rate (j) changes were induced by $PACAP^{PBL \rightarrow DR}$ neuronal activation in a frequency-dependent manner. n = 7 mice per group. Data are presented as the mean ± SEM; see also Supplementary Table 3 for statistical details. $^{**}P<0.01$.

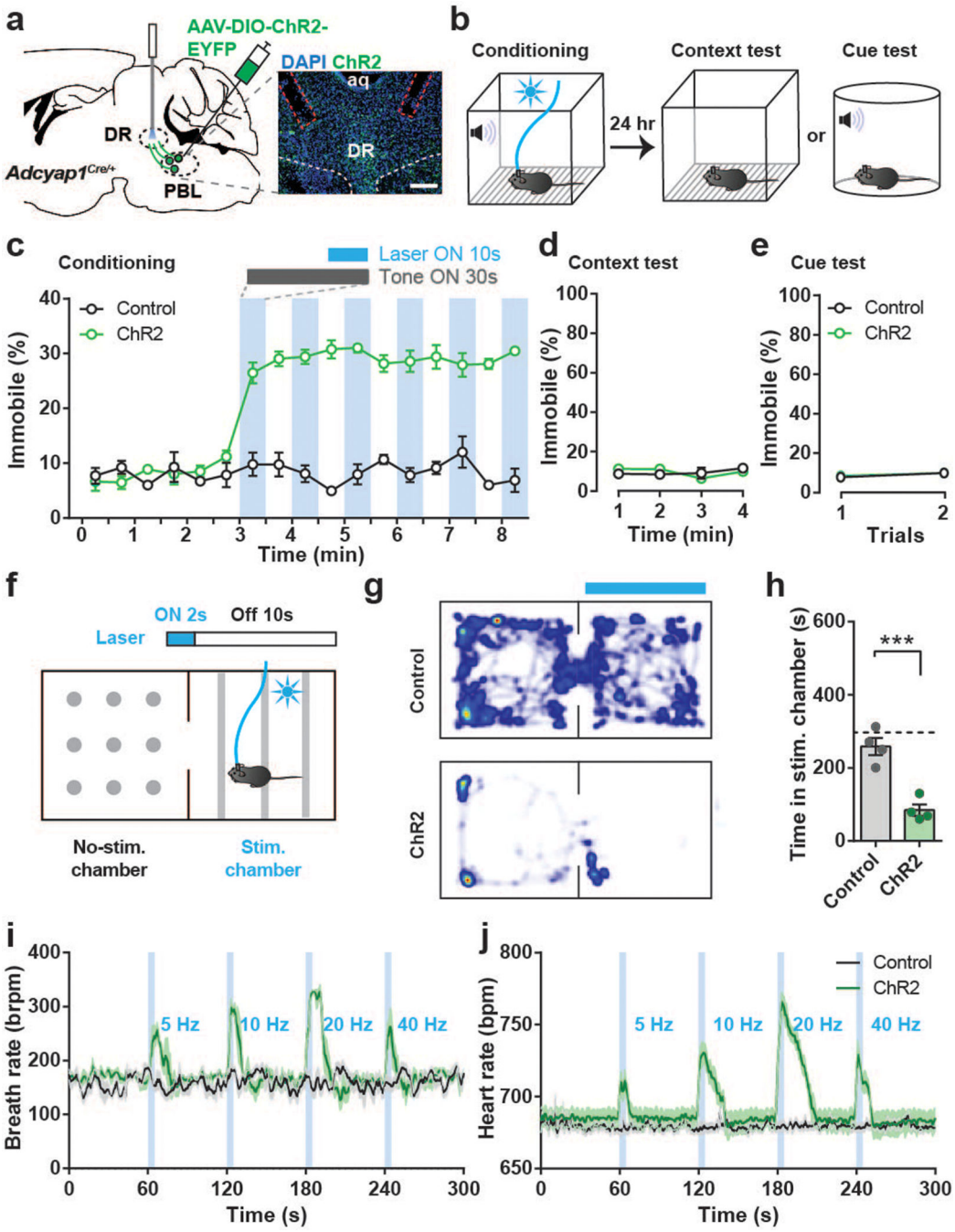

Fig. 4. PACAP$^{PBL\rightarrow DR}$ axon terminal activation produces panic-like symptoms but does not create conditioned fear memory.

a, Schematic and histological confirmation of Cre-dependent expression of ChR2 in the PBL of an *Adcyap1*$^{Cre/+}$ mouse for optogenetic activation of PACAP$^{PBL\rightarrow DR}$ axon terminals. Scale bars: 100 μm. This experiment was repeated on four mice with similar results. **b**, Schematic of optical conditioning test. **c**–**e** Immobility levels during the conditioning (c), context (d), and cue tests (e). n = 4 mice per group. Laser activation is indicated by blue shading. **f**, Schematic of the real-time place aversion test. **g**,**h**, Heat map (g), and time spent

in stimulation-paired and unpaired chambers (h, unpaired two-sided *t*-test, $P = 0.0008$). n = 4 mice per group. **i**,**j**, Breathing (i) and heart rate (j) and corresponding AUC analyses during $PACAP^{PBL \rightarrow DR}$ axon terminal activation (5 sec) at various photostimulation frequencies. AUCs were subtracted from the AUC of the no-stimulation period. n = 4 mice per group. Data are presented as the mean ± SEM; see also Supplementary Table 3 for statistical details. ***$P<0.001$.

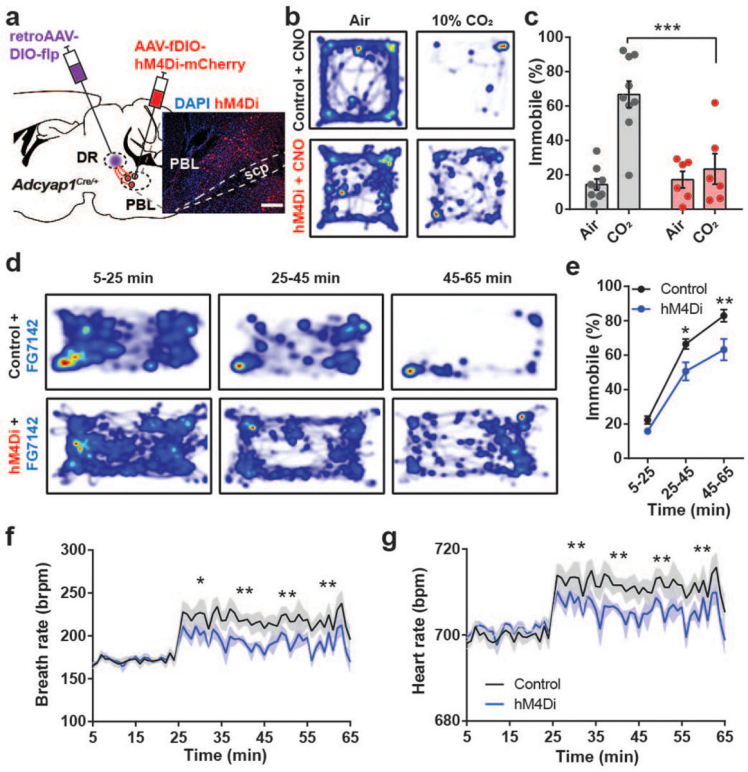

Fig. 5. Inhibition of PACAP$^{PBL\rightarrow DR}$ neurons attenuates panic-like symptoms.

a, Schematic and histological confirmation of Cre- and Flp-dependent expression of hM4Di in the PBL of an *Adcyap1*$^{Cre/+}$ mouse for chemogenetic inhibition of PACAP$^{PBL\rightarrow DR}$ neurons. Scale bars: 100 μm. This experiment was repeated on six mice with similar results. **b**,**c** Representative heat maps of mouse activity (b), and immobile behavior (c, repeated measure two-way ANOVA with Sidak's multiple comparisons test) before (normal air) and after CO_2 exposure during chemogenetic inhibition of PACAP$^{PBL\rightarrow DR}$ neurons. n = 9 control mice, n = 6 hM4Di mice. **d,e**, Representative heat maps of mouse activity (d), and immobile behavior (e, repeated measure two-way ANOVA with Sidak's multiple comparisons test) after FG-7142 injection during chemogenetic inhibition of PACAP$^{PBL\rightarrow DR}$ neurons. n = 9 control mice, n = 5 hM4Di mice. **f,g**, Breathing (f, repeated measure two-way ANOVA with Sidak's multiple comparisons test), and heart rate (g, repeated measure two-way ANOVA with Sidak's multiple comparisons test) changes after FG-7142 injection during chemogenetic inhibition of PACAP$^{PBL\rightarrow DR}$ neurons. n = 9 control mice, n = 5 hM4Di mice. Data are presented as the mean ± SEM; see also Supplementary Table 3 for statistical details. *P<0.05, **P<0.01, ***P<0.001.

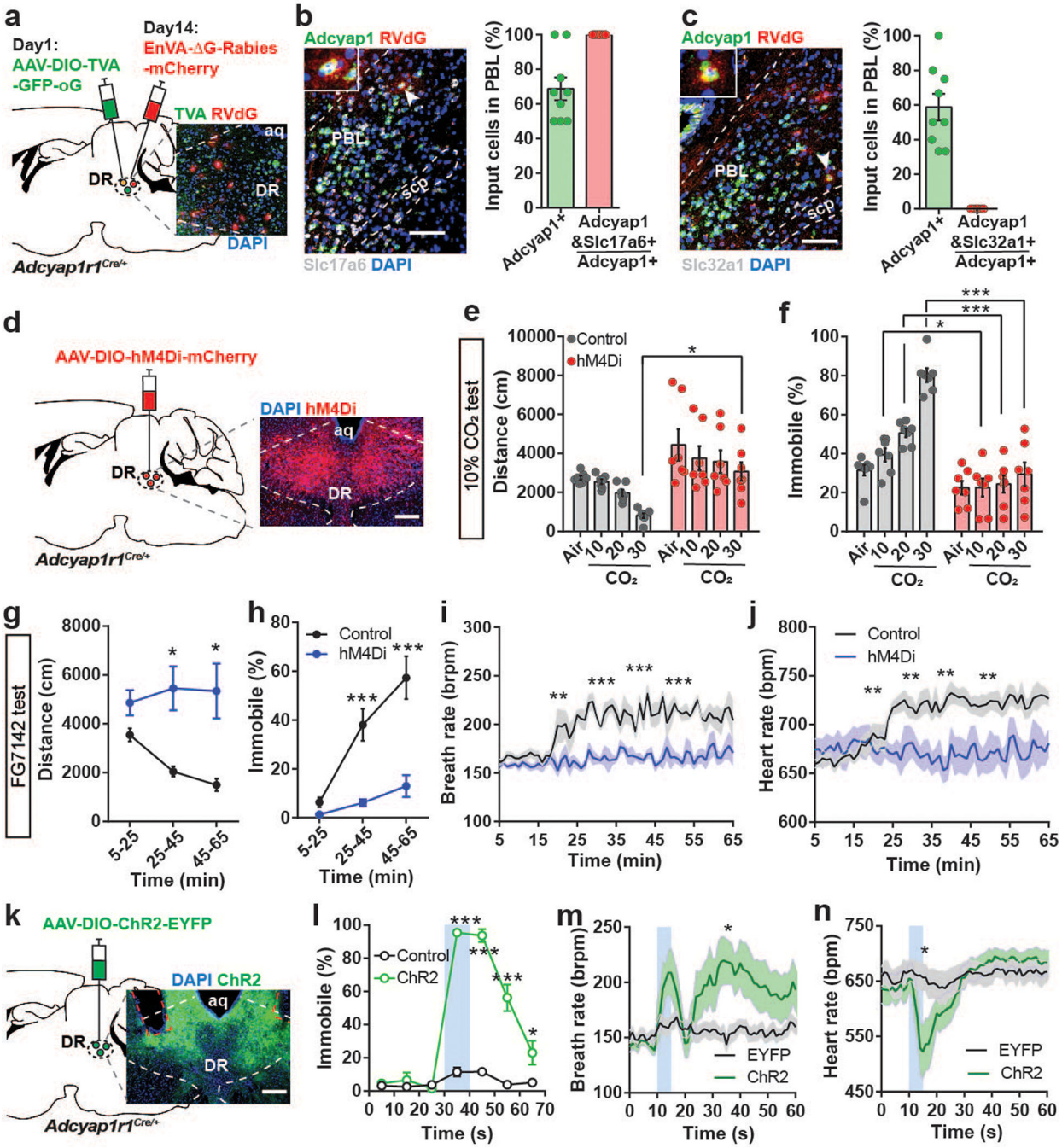

Fig. 6. PAC1R^{DR} neurons receive monosynaptic input from PACAP^{PBL} neurons, and their activation is necessary and sufficient for induction of panic-like symptoms.

a, Schematic and histological confirmation of retrograde rabies tracing of PAC1R^{DR} neurons. **b**, Histological image of RVdG, PACAP (*Adcyap1*), and VGluT2 mRNA (*Slc17a6*) in the PBL (left), with statistical analysis of the presynaptic inputs in PBL (right). The white arrowhead indicates an example of a presynaptic PACAP^{PBL} neuron colocalized with VGluT2. n = 9 slices, 3 mice. **c**, Histological image of RVdG, PACAP mRNA (*Adcyap1*), and VGAT mRNA (*Slc32a1*) in the PBL (left), with statistical analysis of

the presynaptic inputs in PBL (right). The white arrowhead indicates an example of a presynaptic $PACAP^{PBL}$ neuron. n = 9 slices, 3 mice. **d**, Schematic and histological confirmation of Cre-dependent expression of hM4Di in the DR of an *Adcyap1r1*$^{Cre/+}$ mouse for chemogenetic inhibition of $PAC1R^{DR}$ neurons. **e**–**f** Distance traveled (e, mixed-effects analysis with Sidak's multiple comparisons test), and immobile behavior (f, repeated measure two-way ANOVA with Sidak's multiple comparisons test) before (air) and after CO_2 exposure during chemogenetic inhibition of $PAC1R^{DR}$ neurons. n = 7 mice per group. **g,h**, Distance traveled (g, mixed-effects analysis with Sidak's multiple comparisons test), and immobility behavior (h, repeated measure two-way ANOVA with Sidak's multiple comparisons test) after FG-7142 injection during chemogenetic inhibition of $PAC1R^{DR}$ neurons. n = 7 mice per group. **i**,**j**, Breathing (i, repeated measure two-way ANOVA with Sidak's multiple comparisons test), and heart rate (j, repeated measure two-way ANOVA with Sidak's multiple comparisons test) change after FG-7142 injection during chemogenetic inhibition of $PAC1R^{DR}$ neurons. n = 7 mice per group. **k**, Schematic and histological confirmation of Cre-dependent expression of ChR2 and optic fiber placement in the DR of an *Adcyap1r1*$^{Cre/+}$ mouse for optogenetic activation of $PAC1R^{DR}$ neurons. **l**, Photostimulation (10 sec, 40 Hz) induced immediate immobile behavior. Repeated measure two-way ANOVA with Sidak's multiple comparisons test. n = 6 trials/6 EYFP mice, n = 10 trials/5 ChR2 mice. Laser activation is indicated by blue shading. **m**,**n**, Breathing (m, mixed-effects analysis with Sidak's multiple comparisons test), and heart rate (n, mixed-effects analysis with Sidak's multiple comparisons test) changes following photoactivation of $PAC1R^{DR}$ neurons (5 sec, 40 Hz). n = 10 trials/5 mice per group. All scale bars: 100 μm. Data are presented as the mean ± SEM; see also Supplementary Table 1, 3 for counting and statistical details. $*P<0.05$, $**P<0.01$, $***P<0.001$.

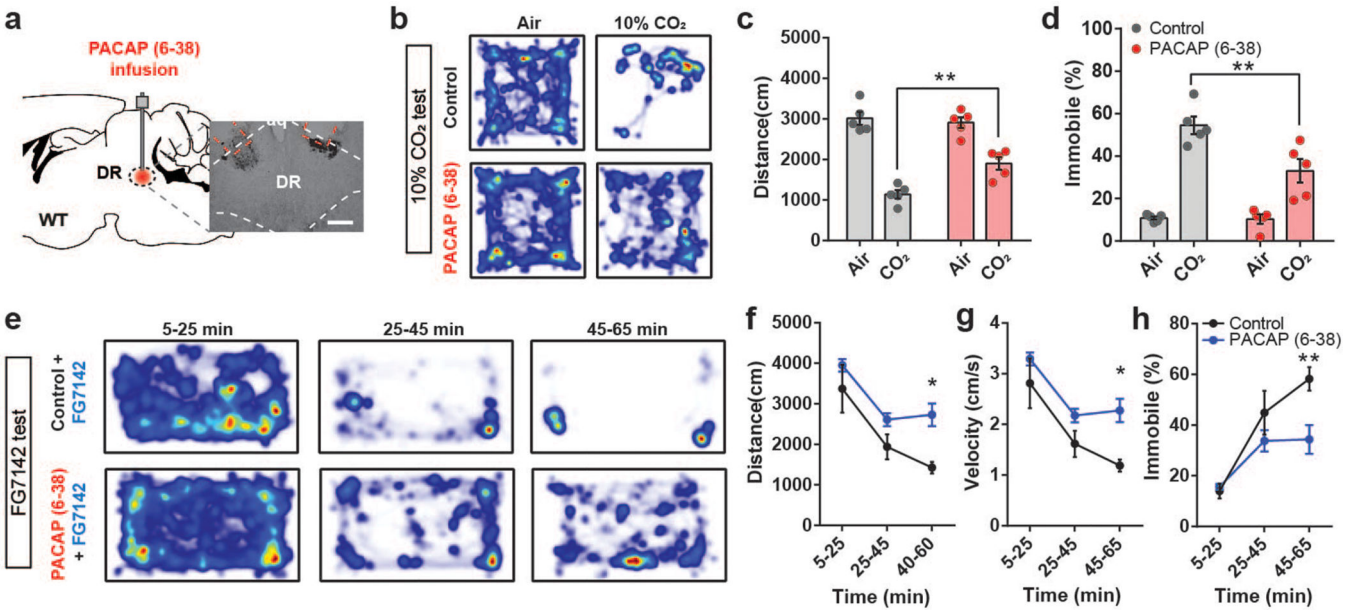

Fig. 7. Infusion of PAC1R antagonist PACAP (6–38) into DR attenuates panic-like symptoms.

a, Schematic and histological confirmation of cannula implantation into the DR of WT mouse for infusion of PAC1R antagonist PACAP (6–38). Scale bars: 100 μm. This experiment was repeated on five mice with similar results. **b**–**d** Heat map of mouse activity (b), distance traveled (c, repeated measure two-way ANOVA with Sidak's multiple comparisons test), and immobility behavior (d, repeated measure two-way ANOVA with Sidak's multiple comparisons test) before (air) and after CO_2 exposure following PACAP (6–38) infusion. n = 5 mice per group. **e**–**h** Representative heat maps of mouse activity (e), distance traveled (f, repeated measure two-way ANOVA with Sidak's multiple comparisons test), velocity (g, repeated measure two-way ANOVA with Sidak's multiple comparisons test), and immobility behavior (h, repeated measure two-way ANOVA with Sidak's multiple comparisons test) after FG-7142 injection and PACAP (6–38) infusion. n = 5 mice per group. Data are presented as the mean ± SEM; see also Supplementary Table 3 for statistical details. *P<0.05, **P<0.01.